(12) LEVEL II

NOSC

AD A105665

Technical Report 696

ELECTRO-OPTICAL ATMOSPHERIC TRANSMISSION EFFORT IN THE MARINE ENVIRONMENT

DTIC
S ELECTE D
OCT 1 6 1981
B

Juergen H. Richter
Herbert G. Hughes

12 May 1981

Prepared for
Naval Material Command
(MAT 0724)

**NAVAL OCEAN SYSTEMS CENTER
SAN DIEGO, CALIFORNIA 92152**

8 1

(14) NOSC/ ... 696

REPORT DOCUMENTATION PAGE		READ INSTRUCTIONS BEFORE COMPLETING FORM
1. REPORT NUMBER NOSC Technical Report 696 (NOSC TR 696)	2. GOVT ACCESSION NO. ADA105665	3. RECIPIENT'S CATALOG NUMBER
4. TITLE (and Subtitle) ELECTRO-OPTICAL ATMOSPHERIC TRANSMISSION EFFORT IN THE MARINE ENVIRONMENT		5. TYPE OF REPORT & PERIOD COVERED Interim FY78–FY81
		6. PERFORMING ORG. REPORT NUMBER
7. AUTHOR(s) J. H. Richter H. G. Hughes		8. CONTRACT OR GRANT NUMBER(s)
9. PERFORMING ORGANIZATION NAME AND ADDRESS Naval Ocean Systems Center San Diego, CA 92152		10. PROGRAM ELEMENT, PROJECT, TASK AREA & WORK UNIT NUMBERS 62759N, F59551, ZF59551002, 532-MP33H
11. CONTROLLING OFFICE NAME AND ADDRESS Naval Material Command (MAT 0724)		12. REPORT DATE 12 May 1981
		13. NUMBER OF PAGES 52
14. MONITORING AGENCY NAME & ADDRESS(if different from Controlling Office)		15. SECURITY CLASS. (of this report) Unclassified
		15a. DECLASSIFICATION DOWNGRADING SCHEDULE

16. DISTRIBUTION STATEMENT (of this Report)

Approved for public release; distribution unlimited

17. DISTRIBUTION STATEMENT (of the abstract entered in Block 20, if different from Report)

18. SUPPLEMENTARY NOTES

19. KEY WORDS (Continue on reverse side if necessary and identify by block number)

Electro-optics
Atmospheric transmission
Marine environment
Aerosol distributions
Aerosol propagation

20. ABSTRACT (Continue on reverse side if necessary and identify by block number)

The electro-optical (EO) atmospheric transmission effort is coordinated among the services in the Department of Defense (DoD), and specific goals and a time frame for their accomplishment have been established. This report reviews the Navy's effort and addresses accomplishments, status, and future plans in the area of systems performance modeling, climatologies, modeling of aerosol distributions, aerosol propagation effects, and instrumentation.

DD FORM 1473 EDITION OF 1 NOV 65 IS OBSOLETE
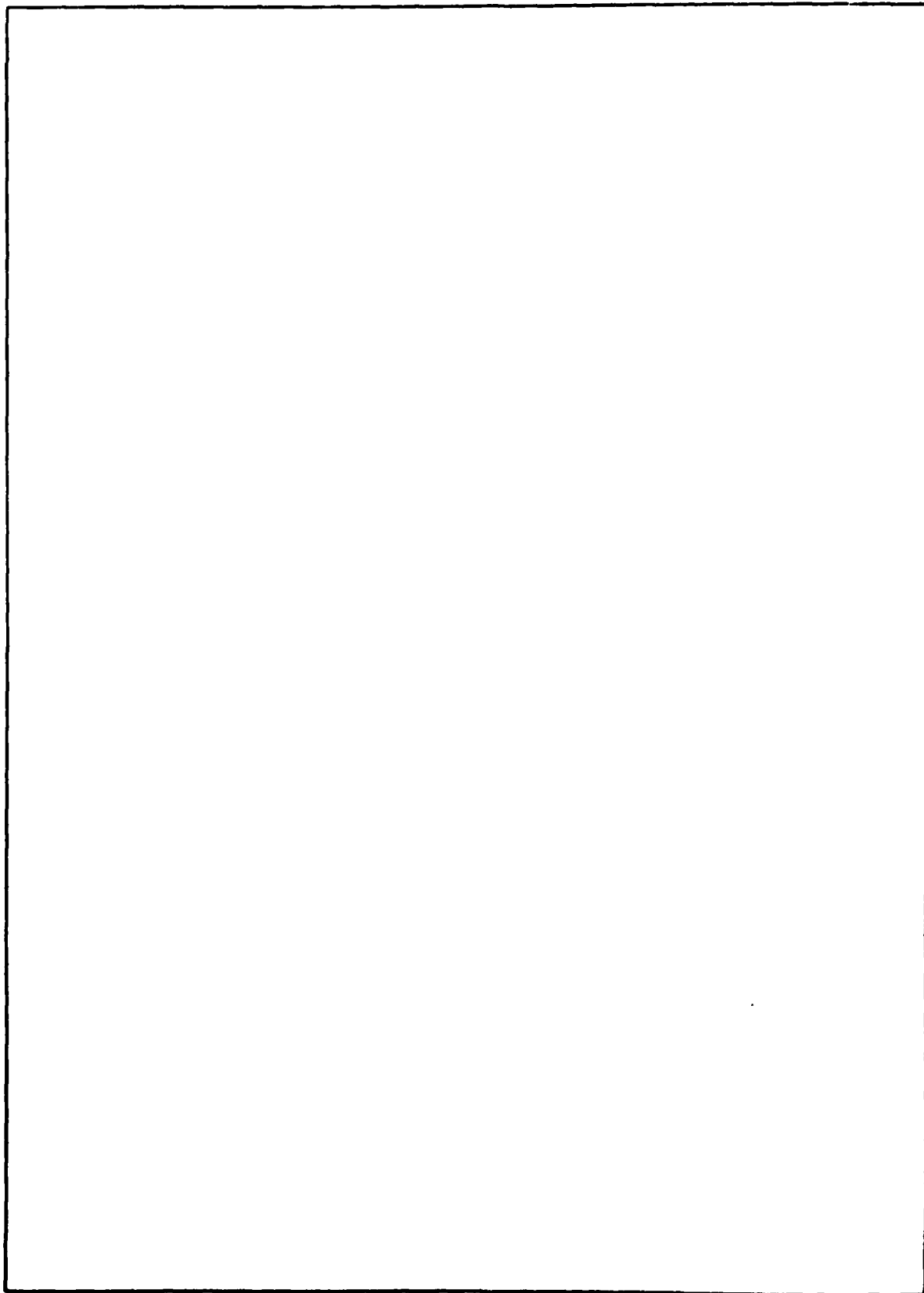1 JAN 73
S/N 0102-LF-014-6601

PROBLEM

Review the Navy's effort and address accomplishments, status, and future
plans in the electro-optical atmospheric transmission areas of systems
performance modeling, climatologies, modeling of aerosol distributions,
aerosol propagation effects, and instrumentation.

RESULTS

The Navy's EO atmospheric transmission program has yielded significant
results in the areas of systems performance assessment, worldwide climatolo-
gies, aerosol measurement and modeling, and instrumentation development.
Future effort will continue in these areas, with an increased emphasis on
development of instrumentation for the operational assessment of the propaga-
tion environment.

CONTENTS

3/4

1.0 INTRODUCTION

The broad objective of the DoD atmospheric transmission effort is to provide the ability to measure, model, and predict atmospheric transmission effects on sensor and communications systems. The Navy's effort concentrates on measurement and modeling of propagation conditions affected by the marine environment. Specific goals are as follows:

1. Relate atmospheric transmission effects to sensor system performance.

2. Accurately model the propagation effects of naturally occurring and manmade aerosols.

3. Relate the production, transport, and dissipation of naturally occurring aerosols to measurable or predictable meteorological parameters.

4. Accurately model the propagation effects of atmospheric molecular absorption.

5. Assess the performance of weapons systems based on validated propagation models applied to historical or derived standard meteorological measurements or models.

6. Develop atmospheric sensor systems to support EO systems operations.

The major areas of the six goals are as follows:

Goal 1: (a) identification, prioritization, and selection of Navy systems; (b) identification of critical atmospheric parameters, sensitivity, and analyses; (c) definition of sensing requirements; (d) examination of climatologies; (e) assessment of sensor systems performance for systems development (simulation) and assessment of shipboard performance (real time).

Goal 2: (a) simultaneous measurements of transmission and aerosols in open ocean and coastal environments; (b) establishment of aerosol refractive indices; (c) validation and improvement of aerosol models; (d) derivation of aerosol extinction scaling laws.

Goal 3: (a) use surface-layer micrometeorological techniques for determination of vertical aerosol distributions; (b) relate marine boundary-layer meteorological parameters (T, RH, W, VIS, etc) to aerosol distributions; (c) conduct aerosol measurements in surface layer (fixed installations and shipboard measurements); (d) use satellite data to infer and forecast aerosol concentrations.

Goal 4: (a) investigation of molecular absorption in specific spectral bands of Navy interest; (b) high- and low-resolution measurements and model verification.

Goal 5: (a) identification of weapon systems; (b) data acquisition in joint programs [Optical Signatures Program (OSP), High Energy Laser Program (HEL)]; (c) improvement and development of atmospheric effects portions of weapon performance models; (d) HEL atmospheric support; (e) spectral band tradeoff analyses; (f) examination of hybrid (modular) systems; (g) examination of countermeasures.

Goal 6: (a) use results from Goal 1 for sensor specification; (b) evaluate point sensing techniques; (c) determine ship influences on point measurement techniques; (d) develop single-ended remote sensors for the measurement of aerosol extinction, molecular absorption, turbulence, and cross wind.

In the following sections, accomplishments, status, and future plans of the Navy's effort in support of the above goals are highlighted. Goals 1 and 5 are combined in the chapter on systems performance modeling. Goals 2 and 3 are jointly described in the chapter on modeling of aerosol distributions and their propagation effects. The effect of molecular absorption (goal 4) is the primary responsibility of the Air Force (Geophysics Laboratory) and has received only limited attention in the Navy program. With the exceptions of

the operation of a Barnes transmissometer at San Nicolas Island (SNI), its comparison with a high-resolution spectrometer, and some analyses pointing toward problems with LOWTRAN in the 4—5-μm band, no Navy effort or accomplishments can be reported. Finally, the section on instrumentation (goal 6) describes the development of direct and remote sensors for the measurement of various atmospheric parameters important to EO transmission.

2.0 SYSTEMS PERFORMANCE MODELING

Systems performance modeling and assessments, as defined in goals 1 and 5, are the ultimate purpose of the entire atmospheric transmission effort. Their accomplishment, however, depends on results from other goals; ie, the development and validation of appropriate models describing the environment. Modeling requirements, their accuracy, and validation are in turn dependent on what systems are to be addressed. Therefore, the process of accomplishing the goals is iterative.

2.1 SENSITIVITY ANALYSES

As a starting point for the Navy's effort, a sensitivity analysis was initiated under the leadership of the Navy Surface Weapons Center. The work concentrated on forward-looking infrared (FLIR) systems, and both parametric and statistical analyses were used. The statistical studies were based on marine weather observations taken by weatherships and reports from passing ships. An example is presented in figure 1, which shows the seasonal statistics for the total extinction coefficient in the 8—12-μm band for weathership J (North Atlantic) and the Mediterranean. Statistical information of this nature may be combined with FLIR performance characteristics (eg, figure 2) to produce the detection range versus geographic region displays shown in figure 3. Two near-term FLIRs are compared, one in the 3.4—5-μm band, the other in the 8—12-μm band. The percentage numbers indicate the percentage of time the detection range is exceeded. This analysis shows larger detection ranges in the lower latitudes for the 3.4—5-μm FLIR and slightly larger detection ranges in the high latitudes for the 8—12-μm FLIR. The physical explanation for this conclusion is that molecular absorption, a chief contribution to extinction in the 8—12-μm band, is high in the tropics because of high humidities. Higher

7

PROBABILITY OF DISTRIBUTION FOR TOTAL EXT COEFF 8-12 µm

WD J SP X
WD J SU ·
WD J FA Y
WD J WI Z

SEASONAL STATISTICS FOR MEDITERRANEAN

WD 2 SP X
WD 2 SU ·
WD 2 FA Y
WD 2 WI Z

PROB. OF EQUALING OR EXCEEDING ABCISSA

TOTAL EXT COEFF (km⁻¹)

Figure 1. Seasonal statistics for the total
extinction coefficient in the 8—12-µm band for
weather ship J (North Atlantic) and the
Mediterranean.

WFOV 8-12 µm FLIR

.30 KM ALT
X--CG
*--NT
Y--FT

TOTAL EXTINCTION COEFFICIENT/KM

WFOV 8-12 µm FLIR

.02 KM ALT
X--CG
*--NT
Y--FT

TOTAL EXTINCTION COEFFICIENT/KM

Figure 2. Detection range versus extinction
coefficient for a wide field of view (WFOV)
8—12-µm FLIR (CG = current generation; NT =
near term; FT = far term) at 300-m and 20-m
altitudes.

8

aerosol concentrations in high latitudes affect the 3.4—5-μm band more than the 8—12-μm band accounting for the reversal of performance of the two FLIRS. The analysis was based on the aerosol model in LOWTRAN 3B, which has a 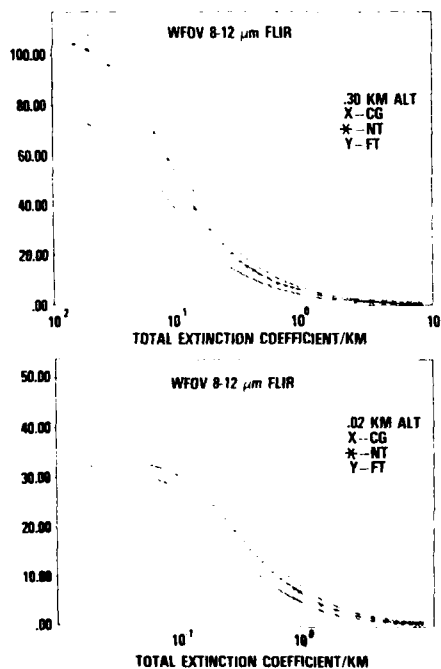number of shortcomings, as discussed in section 3. The same analysis was performed by using a modification of the Wells et al (1977) model by Katz and Ruhnke (K/R); the result is shown in figure 4. The basic conclusion concerning the relative performance of the two FLIRs as a function of geographic region remains unchanged. However, the absolute detection range values obtained from the different aerosol models showed significant differences. This emphasized the need for the aerosol model development and validation effort described in section 3.

The generation of performance curves of figures 3 and 4 requires a significant computational effort if one deals with band averages in atmospheric transmission bands for which the extinction coefficient becomes range-dependent. Figure 5 illustrates the range dependency of molecular absorption coefficients. To reduce the computational effort in generating range-dependent systems performance curves, the statistical weather information was plotted as a function of atmospheric transmission with range as a parameter. Figure 6 is an example for weathership J in summer and the 8—12-μm band. From this display, atmospheric transmission as a function of the atmospheric path with probability of occurrence as a parameter can be plotted as shown in figure 7 for the 3.4—5-μm and the 8—12-μm bands. On the same graphs, the performance characteristics for various FLIRs can be overlaid. The intersections between the FLIR performance and the atmospheric transmission curves provide the data points needed for presentations of figures 3 and 4. This procedure has greatly speeded up the process of evaluating statistical systems performance and has contributed to the support of a number of system evaluations. Examples of EO systems support provided include, besides FLIRs, the optical fire-control portion of SEAFIRE; infrared search and track sets

---

Wells, W.C., G. Gal, and M. W. Munn (1977): Aerosol distributions in maritime air and predicted scattering coefficients in the infrared, Appl Opt, 16, pp 654-659.

NEAR TERM 3.4-5 μm & 8-12 μm WFOV FLIRS
DETECTION RANGE VS LATITUDE
20, 50, AND 80% CUMULATIVE PROBABILITY POINTS
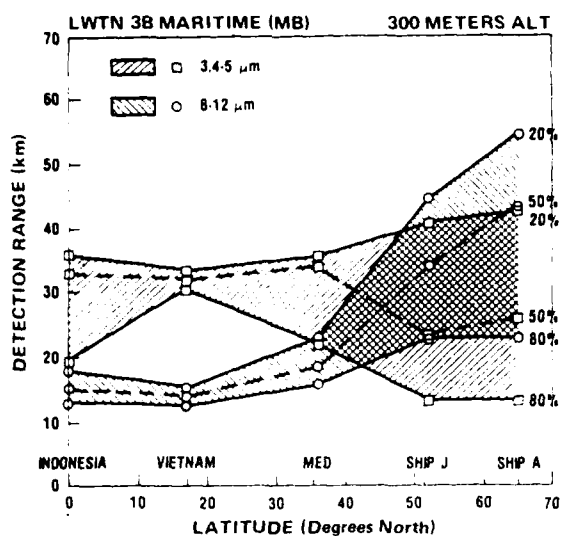
LWTN 3B MARITIME (MB)   300 METERS ALT

Figure 3. Detection range versus latitude for
3.4—5-μm and 8—12-μm wide-field-of-view FLIRs.
The percentage numbers on the lines indicate
the percentage of time detection range is
exceeded.

K/R AEROSOL MODEL   300 METERS ALT

Figure 4. Same analysis as in figure 3, but using
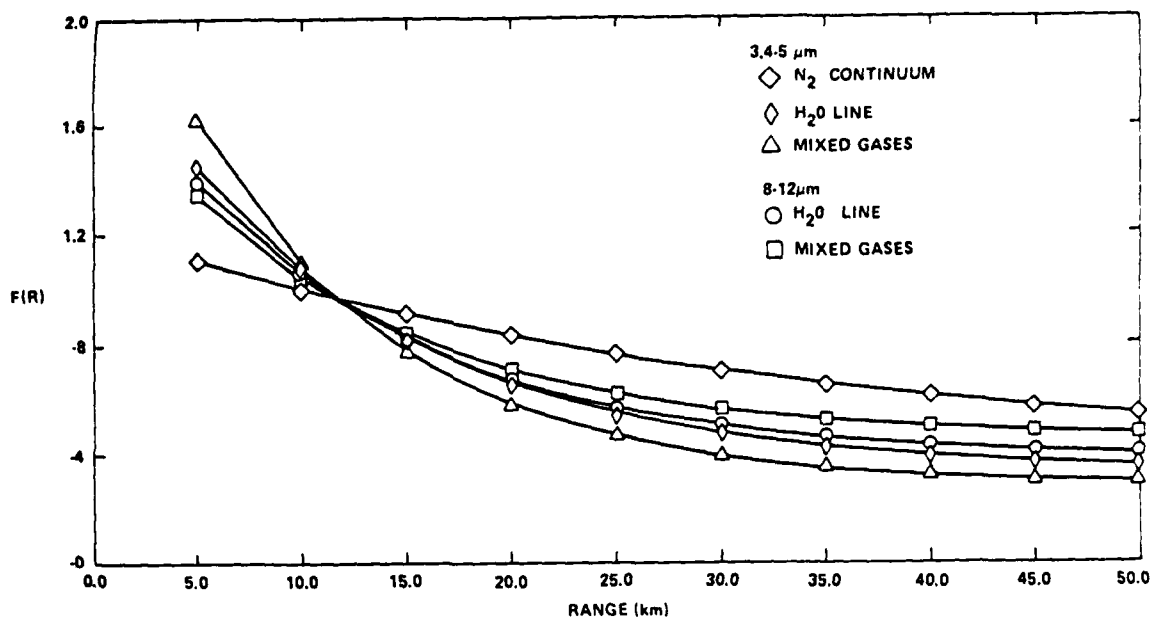a different aerosol model (K/R = Katz/Ruhnke
model).

10

Figure 5. Range dependency of molecular
absorption coefficients derived from LOWTRAN 3B
for wavelength-averaged effective exponential
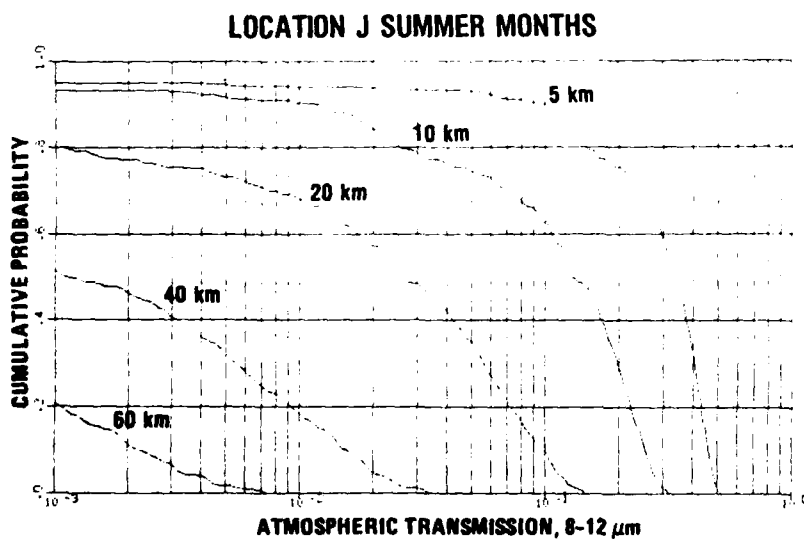transmission function F(R). [F(R) values are
approximately unity at 10 km.]

Figure 6. Cumulative probability of transmission
in the 8—12-µm band with range as parameter for
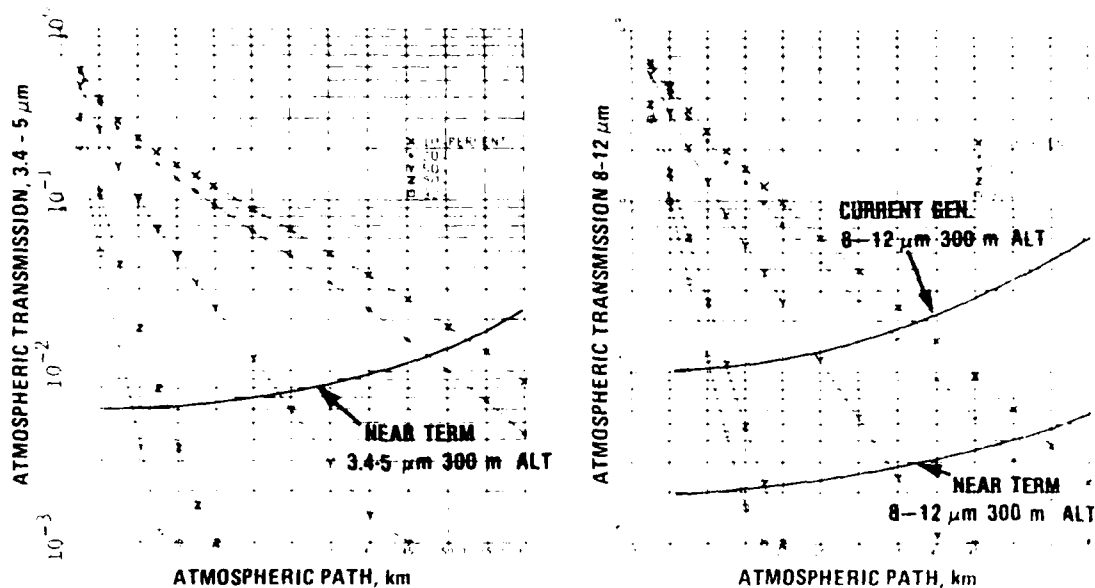weather ship J in summer.

11

Figure 7. Cumulative probability of transmission
versus range for weather ship J in summer and
performance characteristics for three different
FLIRs.

(IRST), which are nonimaging surveillance systems; laser-guided ordnance;
infrared guided projectiles; and laser rangefinders.

Considerable effort has been spent on verification of various modeling
aspects. The Navy's transmission facility at San Nicolas Island (SNI) has
provided an extensive body of simultaneous transmission and meteorological
data. The SNI transmissometer analysis was particularly useful in evaluating
molecular codes and aerosol wind-speed effects. These efforts are described
in more detail by Katz and DeBold (1981). Future plans in the area of sensi-
tivity analyses include laser and slant path sensitivity studies, laser range-
finder illumination studies, FLIR and IRST performance modeling, continuation
of the evaluation of the SNI transmission and meteorological data, the

Katz, B. S., and F. C. DeBold (1981): A statistical evaluation of optical
propagation codes using 1978 San Nicolas Island transmissometer measurements,
Proc 29th National IRIS Symposium, Orlando, FL, 19-21 May.

12

incorporation of the latest models described in section 3, and incorporation
of variable ship signatures and unresolved air targets.

2.2 REAL TIME ASSESSMENT

The performance of any deployed Navy EO system should be assessable under
operational conditions. That this can be done successfully for a shipboard
environment for sensors affected by meteorological parameters has been
demonstrated for radar and communications by the Integrated Refractive Effects
Prediction System (IREPS) (Hitney and Richter, 1976; Hitney and Paulus, 1979).
This system is presently operational on all deployed US aircraft carriers and
utilizes a Hewlett Packard 9845 desktop calculator. The environmental inputs
are provided by radiosondes, surface measurements, and sensors flown on air-
craft. Combined with the stored electromagnetic parameters, IREPS provides in
near real time radar coverage diagrams, systems propagation loss diagrams, and
other displays or tables which give the operator performance data for the
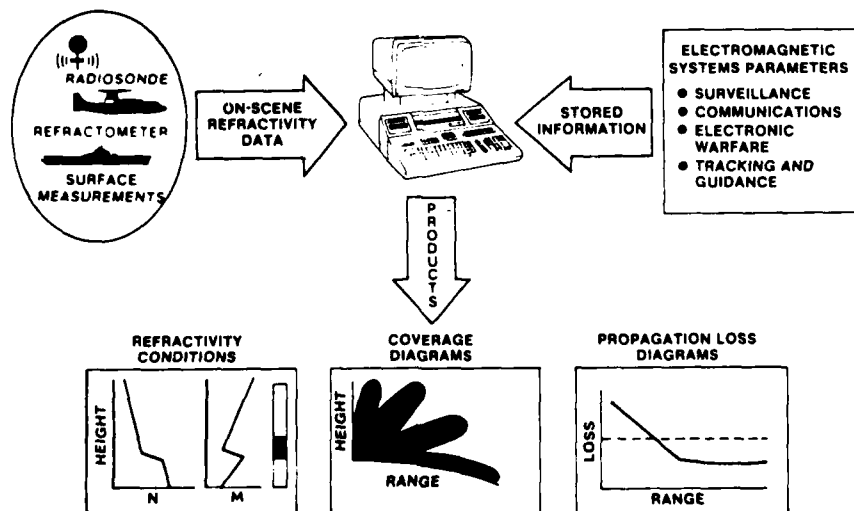environmental conditions encountered (figure 8). For the same hardware that

Figure 8. Integrated Refractive Effects
Prediction System (IREPS).

Hitney, H. V., and J. H. Richter (1976): Integrated Refractive Effects
Prediction System (IREPS), Naval Engineers Journal, pp 257-262, April.

Hitney, H. V., and R. A. Paulus (1979): Integrated Refractive Effects
Prediction System (IREPS), interim user's manual, NOSC TD 238, March.

IREPS uses, an EO module has been designed which is called PREOS (Performance and Range for EO Systems) (Snyder, 1980). Figure 9 shows the general graphic display format for PREOS. The operator specifies location, target, environmental data, and task choices, and receives a display for the selected system. An example for an airborne FLIR is presented in figure 10. In the upper portion of the figure, a table provides detection or identification ranges for various targets as a function of altitude. The same information is displayed in graphical form below the table. Various models are available to calculate the FLIR performance. Figure 11 compares ranges calculated from three different models. The first calculates FLIR performance based on one humidity value and assuming standard vertical lapse rates. This can lead to serious range errors if vertical humidity gradients are present. The profile used for the comparison has a 70% change in humidity at an altitude of 800 feet. In the first model, this leads to a serious overestimate in range when the FLIR is above the moist layer and predictions are based on humidity values at this altitude. Both the second and third model do account for the actual vertical humidity structure. Their main difference is that, for NOSC model 1, empirically determined detection ranges for the various targets encountered are used; NOSC model 2 calculates detection ranges based on temperature differences between target and background. A possible explanation for the significant detection range differences, in particular for small targets, is that detection may be enhanced by a wake. To settle the differences between the various models, an extensive model evaluation effort is presently underway. This effort consists of making target spectral radiant intensity measurements by using a high-quality calibrated thermal imaging system flown in a helicopter (as shown in figure 12) and collecting simultaneous meteorological data. In a separate effort, operational FLIR performance data, together with appropriate meteorological data, are gathered by an S-3A

Snyder, F. P. (1980): PROCAL-PREOS: A fast running airborne FLIR system performance model, NOSC TN 810, 15 Feb.

Figure 9.   Display format for PREOS.

Figure 10.   Airborne FLIR performance assessment
provided by PREOS.

15

Figure 11. Comparison of three different models to calculate FLIR performance ranges.

$$\beta_\lambda = -\,d/dR\left\{\ell n\,(E_\lambda R^2)\right\}$$

HELICOPTER MOUNTED
THERMAL IMAGING SYSTEM

R_3

R_2

R_1

$\ell n\,(E_\lambda R^2)$

R

TARGET SPECTRAL RADIANT
INTENSITY E_λ MEASURED AT
DIFFERENT RANGES R

Figure 12. PREOS FLIR performance model evaluation.

squadron (FLIR-equipped antisubmarine warfare aircraft). The results from
both efforts should validate the model to be used in PREOS.

2.3 EO CLIMATOLOGIES

Performance modeling of EO systems as a function of season and geographic
area requires the availability of good EO climatologies. Consequently, the
compilation of such climatologies has been an important part in the Navy's
atmospheric transmission effort. Examples of surface optical and slant path
parameters have been given previously. Surface climatologies have been
completed for all weather ships. Estimates of the probability of cloud-free
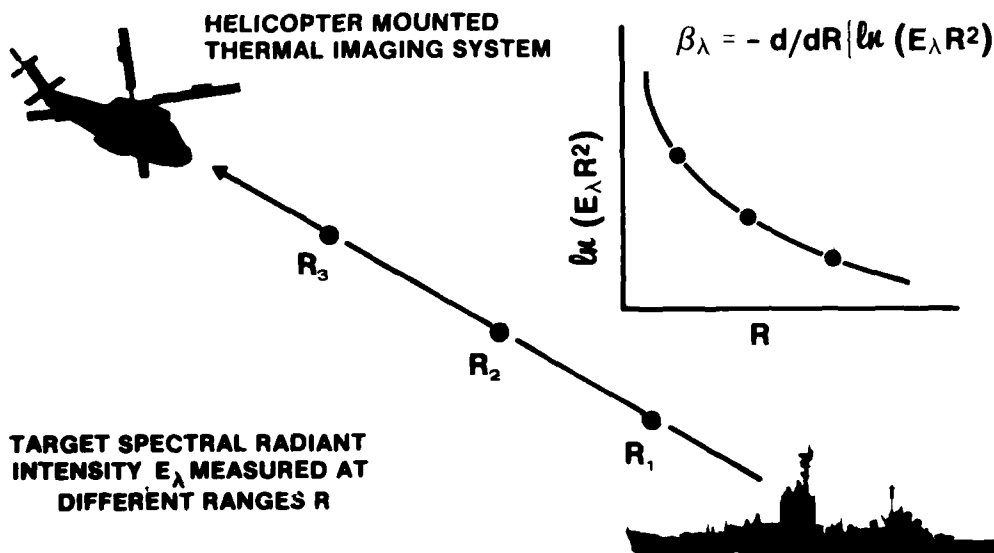line-of-sight (PCFLOS) were calculated for a set of nine angles by using a
modification of Lund and Shanklin's universal method from lower cloud weather
data taken at fifteen marine locations. The data compilation covers periods
from 5 to 7 years (1964-1971) and provides statistics for seasonal variations
of lower cloud base heights and cover as well as low cloud type and cover
(Katz et al, 1981). Examples of this effort are shown in figures 13 and 14.
Figure 13 shows cloud base height statistics for weathership M for summer and
figure 14 the probability of cloud-free line of sight to various altitudes as
a function of elevation angle for weathership M for three seasons. In a
related effort, CFLOS probabilities are derived from the Air Force Global
Weather Central's automated cloud analysis model (3DNEPH) for 28 ocean areas
in the Northern Hemisphere (eg, deViolini et al, 1980).

Future plans in the climatology effort include incorporation of updated
models, as described in the next section, and publication of climatology
atlases (area climatologies) for surface and slant path geometries.

Katz, B. S., F. C. DeBold, and J. J. Perez-Esaudi (1981): Estimates for the
probabilities of surface-to-air cloud free lines-of-sight and low cloud
statistics at fifteen marine locations from surface observations, NSWC TR
78-143.

deViolini, R., A. Shlanta, and C. B. Elam (1980): Seasonal cloud amount and
cloud free line-of-sight data for the oceanic area off the Somali Coast, PMTC
TP 80-19, July.

Figure 13.   Cloud base height statistics for
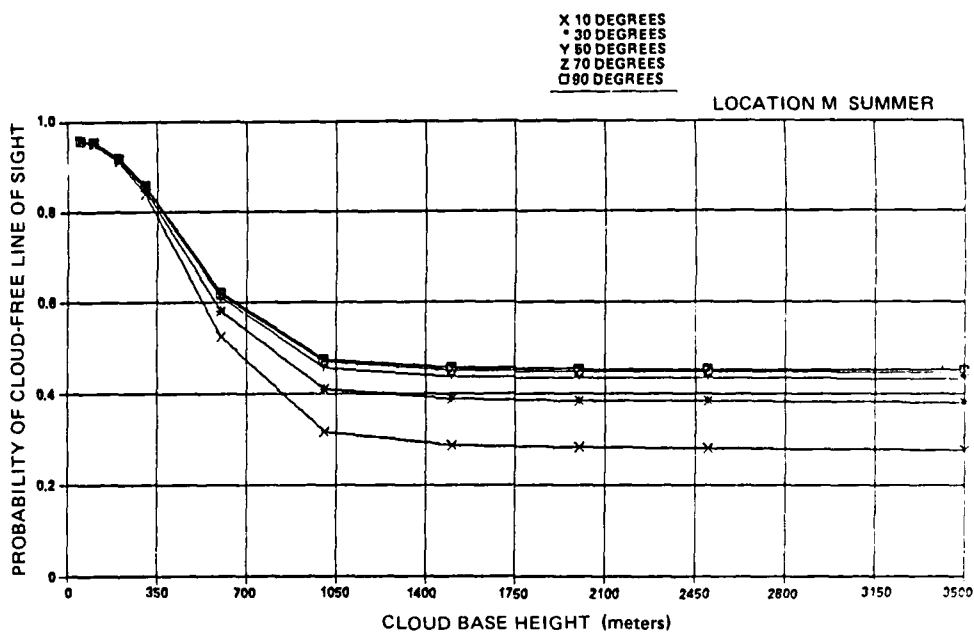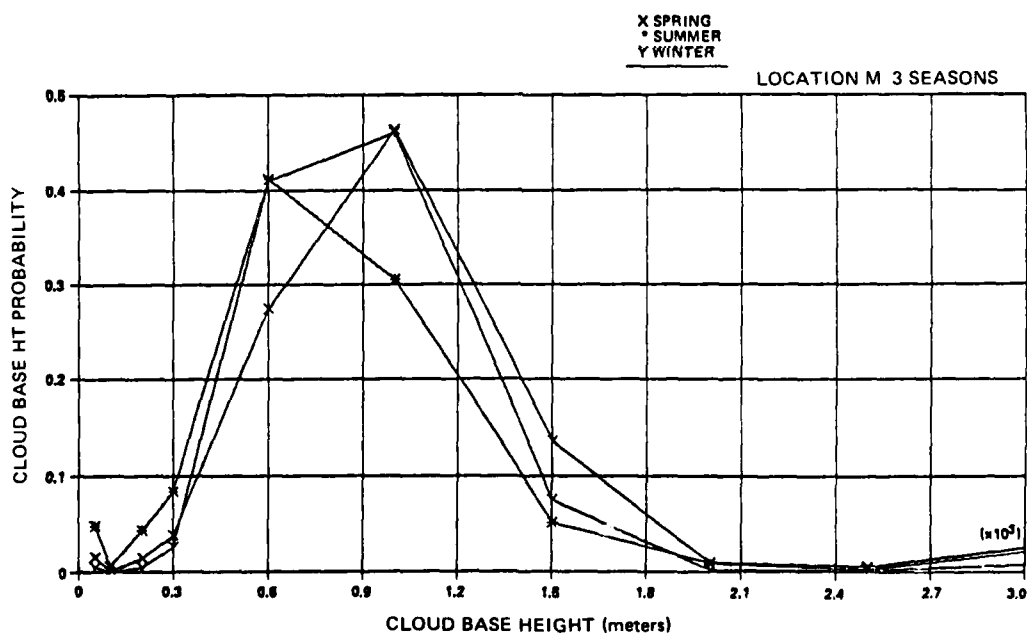weather ship M for summer.

X SPRING
* SUMMER
Y WINTER

LOCATION M 3 SEASONS

Figure 14.   Probability of cloud-free line of
sight to various altitudes as a function of
elevation angle for weather ship M for three
seasons.

3.0 MODELING OF AEROSOL DISTRIBUTIONS AND THEIR PROPAGATION EFFECTS

3.1 DESCRIPTION OF AEROSOL MODELS

Analytical models of aerosol size distributions based on measurable meteorological parameters are of primary importance in the prediction of electro-optical systems performance at sea where transmission or particle size measurements cannot be easily made. Given the appropriate analytical model of the size distribution and the aerosol effective index of refraction, extinction coefficients at the wavelengths of interest can be calculated by using Mie theory.

In recent years, two-component (continental and maritime) empirical models of aerosol size distributions have emerged from which infrared (IR) extinction coefficients can be calculated. In the model of Barnhardt and Streete (1970), the continental component is described by a Junge (1955) distribution and the maritime component is described by the modified gamma distribution used by Deirmendjian (1969). Included in the model are the effects of relative humidity on the size distribution and the refractive indices of the particles. In the model of Selby et al (1976) (hereafter referred to as the LOWTRAN 3B maritime model), the continental and maritime components are represented by log-normal distributions with the maritime component contributing 75% of the extinction at 0.55 μm. In the LOWTRAN 3B approach, the particle size distribution is assumed to be constant with altitude and the aerosol extinction coefficients as a function of wavelength

Barnhardt, E. A., and J. C. Streete (1970): A method for predicting atmospheric aerosol scattering coefficients in the infrared, Applied Optics, 9, 1337-1344.

Junge, C. (1955): The size distribution and aging of natural aerosols as determined from electrical and optical data of the atmosphere, J Meteor, 16, pp 654-659.

Deirmendjian, D. (1969): Electromagnetic Scattering on Spherical Poly-dispersions, Elsevier.

Selby, J. E. A., E. P. Shettle, and R. A. McClatchey (1976): Atmospheric transmittance from .25 to 28.5 m: Supplement LOWTRAN 3B, AFGL-TR-86-0258.

are precalculated by using the "oceanic" indices of refraction and then are normalized to an observed surface visibility of 23 km, which includes the contributions from Rayleigh scattering. The total number density of particles is allowed to vary exponentially with altitude from a value at the ground based on surface visibility. This procedure allows the extinction coefficient variation with altitude to be scaled from surface visibility measurements, but maintains a constant ratio of visible-to-IR extinction with altitude. While the relative humidity and wind speed are not explicit to the model, the distribution is supposed to correspond to a relative humidity of 80% and moderate wind speeds. More recently, this model has been improved upon in LOWTRAN 5 (Kneizys et al, 1980) to include the effects of relative humidity and its variation with altitude.

The effects of surface wind velocity and relative humidity variation with altitude were included in the model of Wells et al (1977) (hereafter referred to as the WGM model). In this model, the continental and maritime representations of Barnhardt and Streete are maintained, as is the model of aerosol radius growth rate with relative humidity, which assumes the dry particle to be NaCl. In the continental component, the constants of the Junge distribution were adjusted to agree with the work of Barnhardt and Streete for a relative humidity of 80% and a continental-to-maritime mixture ratio of 1:2.5. In the maritime component, the constants of the Deirmendjian distribution were modified to include surface wind speed and relative humidity based on fits to the empirical data. Simple exponential scale heights were also introduced as functions of particle radius which (with relative humidity lapse rates) account for altitude variations. The aerosol size distribution model is given by equation 1.

$$n(r) = \frac{\beta^*}{F'} \left\{ 0.47 \left(\frac{r}{F'}\right)^{-4} \exp(-h/hc) + 0.434\alpha \left(c_1 + c_2 V_s^{\delta}\right) \right.$$

$$\left. \times \left(\frac{r}{F'}\right) \exp\left[-8.5\left(\frac{r}{F'}\right)^{\gamma} - h/hm\right] \right\} \tag{1}$$

Kneizys, F. X., et al (1980): Atmospheric transmittance/radiance: computer code LOWTRAN 5, AFGL-TR-80-0067.

20

where $n(r)$ = number of particles cm^{-3} μm^{-1} (radius)

         r = radius (μm)

         h = altitude (km)

         h_c, h_m = scale heights (km) for the continental and marine components, respectively (listed in tabular form as a function of particle radius and altitude in Wells et al, 1977)

         α = continental to maritime mixing ratio

         F = radius growth factor [$=1 - 0.9 \ln(1-S)$ for $S \geq 0.4$]

         S = saturation ratio

         F' = $F(S)/F(0.8)$

         V_s = surface wind speed (m s^{-1})

$$(C_1 + C_2 v^\delta) = \begin{cases} 250 + 750 \ v_s^{1.16} \ , & v_s < 7 \ m \ s^{-1} \\ 6900 \ v_s^{0.29}, & V_s \geq 7 \ m \ s^{-1} \end{cases}$$

$$\gamma = 0.384 - 0.00293 \ v_s^{1.25}$$

$$\beta^* = \frac{3.912}{R_v \beta_{cal}(0.55 \ \mu m)} \ .$$

In the formulation, β^* is a factor which normaliz the distribution to an observed visual range (visibility) R_v (with Rayleigh scattering removed) and also normalizes the Mie aerosol extinction coefficient $\beta_{cal}(0.55 \ \mu m)$ by using the size distribution prior to normalization. For a given size distribution at the ground, the ratio of visible and IR extinctions is then fixed. However, this ratio will change with altitude, depending on the particle growth with change in the relative humidity.

Using a large data set of meteorological parameters obtained from surface weatherships, B. A. Katz (of the Naval Surface Weapons Center, White Oak, MD)

and L. Ruhnke (of the Naval Research Laboratory, Washington, DC) modified the constants of the original WGM model. In this model (hereafter referred to as the K/R model), the visibility scaling factor was removed because of the unreliable visibilities reported in the data sets. The scale height term in the continental component was also removed, leaving the altitude variations as functions of humidity and exponential scale height in only the maritime component. The growth rate with relative humidity model was also changed from that of Barnhardt and Streete to that of Fitzgerald (1975), which allowed the particle growth rate to vary with differing species of condensation nuclei. The model assumes the aerosols to be at equilibrium with the surrounding medium, and hysteresis effects are neglected. The K/R model is described by equation 2.

$$
n(r) = 1.7 \left(\frac{r}{\alpha} \right)^{-4} + 1.62 \left(C_1 + C_2 v^{\delta} \right) \cdot \exp \left[\frac{-z}{h_o F} - 8.5 \left(\frac{r}{\alpha} \right)^{\Gamma} \right] F^{-1} \left(\frac{r}{\alpha} \right) \qquad (2)
$$

where $n(r)$ = number of particles per cm^3 per μm (radius)

r = radius (μm)

z = altitude (m)

h_o = scale height set at 800 m for $z < 1$ km

α = 0.81 $\exp \left[\frac{0.066S}{1.058 - S} \right]$

S = saturation ratio (relative humidity $\div$ 100)

V = wind factor scaled with surface wind V_o

= 0.5 m/s for $0 \leq V_o \leq 4$ m/s

= $(V_o - 3.5)$ m/s for $V_o > 4$ m/s

F = $1 + (V/60)^3$

Γ = $0.384 - 0.00293 \, v^{1.25}$

when $V \leq 7$ m/s, $C_1 = 350$, $C_2 = 10^3$, $\delta = 1.15$

$V > 7$ m/s, $C_1 = 0$, $C_2 = 6900$, $\delta = 0.29$.

Fitzgerald, J. W. (1975): Approximate formulas for the equilibrium size of an aerosol particle as a function of its dry size and composition and the ambient relative humidity, J Appl Meteor 14, pp 1044-1049.

The empirical models described have been developed from limited sets of surface measurements, and their validity under varying maritime conditions and with altitude have not yet been fully examined. Major objectives of the Navy's electro-optical transmission program have been to establish a data base of simultaneously measured optical transmission, meteorological, and atmospheric aerosol data, and then to make comparisons between (1) aerosol size spectrometers and (2) extinction coefficients calculated by using the modeled distributions, the distributions calculated from the measured sized distributions, and/or those measured by transmissometers. In the following sections, examples and results of model validation attempts on the ground and with altitude are discussed.

3.2 MODEL VALIDATION ATTEMPTS

Primary instruments utilized in the aerosol model validation efforts are aerosol spectrometers manufactured by Particle Measuring Systems, Inc (PMS), which are usually referred to as Knollenberg spectrometer probes (after the inventor and founder of PMS). The instruments are utilized on the ground by several participants in the Navy's program, and also are flown on a twin-engine Piper Navajo aircraft (figure 15) with which spatial measurements are made. The aircraft is also instrumented with air, dewpoint, and sea surface temperature and pressure sensors. Questions as to the accuracy, reproducibility, and usefulness of these probes were raised by several theoreticians and users within the governmental community. These questions prompted an experiment to be conducted during a 2-week period in April and May 1979 at San Nicolas Island (SNI), in which all of the Navy's available Knollenbergs were operated simultaneously during different meteorological conditions. Extinction coefficients calculated from measured size distributions were then compared with transmissometer, interferometer, lidar, polar nephelometer, and horizon contrast photometric measurements. Participants and their areas of responsibility in the cooperative measurement program included:

QUARTZ AIR TEMPERATURE PROBE
AND INTEGRATING NEPHELOMETER
AIR INTAKE

ASSP-100

DEWPOINT
HYGROMETER

OAP-200

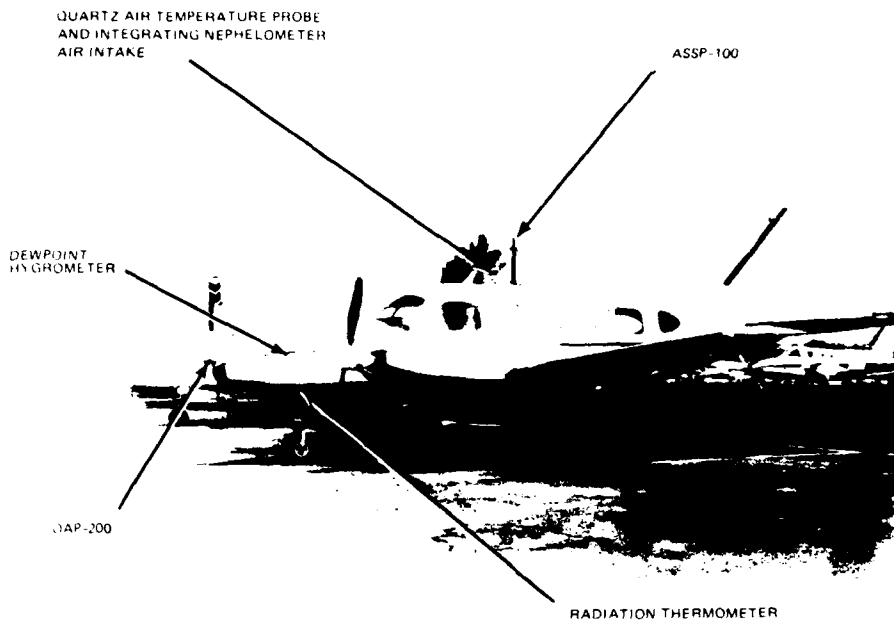RADIATION THERMOMETER

Figure 15. NOSC Knollenberg/meteorological
sensors installation.

1. Naval Ocean Systems Center (NOSC): Surface aerosol size distribution
    measurements; instrumented aircraft for aerosol, air temperature,
    dewpoint, and sea surface temperature measurements.

2. Naval Postgraduate School (NPS): Aerosol size distribution measure-
    ments.

3. Naval Research Laboratory (NRL): High-resolution and broadband
    atmospheric transmittance, aerosol size distributions, visibility,
    baseline meteorology, micrometeorology, aerosol size distributions,
    and radon count.

4. Pacific Missile Test Center (PMTC): Broadband atmospheric transmit-
    tance, baseline meteorology, rawinsondes, and satellite data.

5. Atmospheric Sciences Laboratory, White Sands Missile Range (ASL,
    WSMR): Visibility and laser ranging (visioceilometer).

24

6. Particle Measuring Systems, Inc (PMS): Aerosol size distribution
   measurements.

7. Hansen, Schuler, and Stewart (HSS): Horizon contrast photographs for
   visibility measurements.

8. Aeronautical Research Associates of Princeton (ARAP): Single
   scattering phase functions, aerosol size distributions, ozone
   concentration, and UV transmittance.

The measurement site at SNI is shown in figure 16. This island facility
is under the cognizance of the Pacific Missile Test Center, Point Mugu, CA. A
total of 11 Knollenberg probes were located on a tower (figure 17) at the
receiving site (site A) of a Barnes 14-712 VLR transmissometer, which is
operated over a 4.1-km path (Site C to A) across Laser Bay at the northwest
tip of the island. The results of this intercomparison experiment have been
discussed by Jensen et al. (1980). An example of simultaneously measured
particle size distributions (dN/dr versus radius) for a selected 30-minute
time period on 9 May have been superimposed on each other in figure 18.
Averaged values of air temperature, relative humidity, wind speed, and
visibility are also indicated. Each of the individual spectra show peaks that
do not correlate with each other, and the slopes of the individual spectra
vary from one spectrometer to the other. Differences between the individual
spectra also exceed an order of magnitude. While these differences in size
distributions are large, the extinction coefficients calculated on the basis
of these spectra compare well, as is seen in figure 19. In the figure, the
extinction coefficients (βa) calculated ($\lambda = 1.06$ µm) from the size distribu-
tions measured by the various probes agree within factors of two. However,
for all the measurements, a systematic offset between the calculated extinc-
tions and those measured by the Barnes transmissometer and the Army's visio-
ceilometer was observed, with the calculated values being usually greater by a
factor of two. Aircraft observations along the Barnes optical transmission
path provided insight as to the possible causes of the constant bias. Figure
20 shows the particle number density and the calculated extinction coefficient

Jensen, D. R., R. Jeck, G. Trusty, and G. Schacher (1980): Intercomparison of
PMS particle size spectrometers, NOSC TR 555.

Figure 16. Topographical map of San Nicolas Island showing optical propagation range on northwest tip.
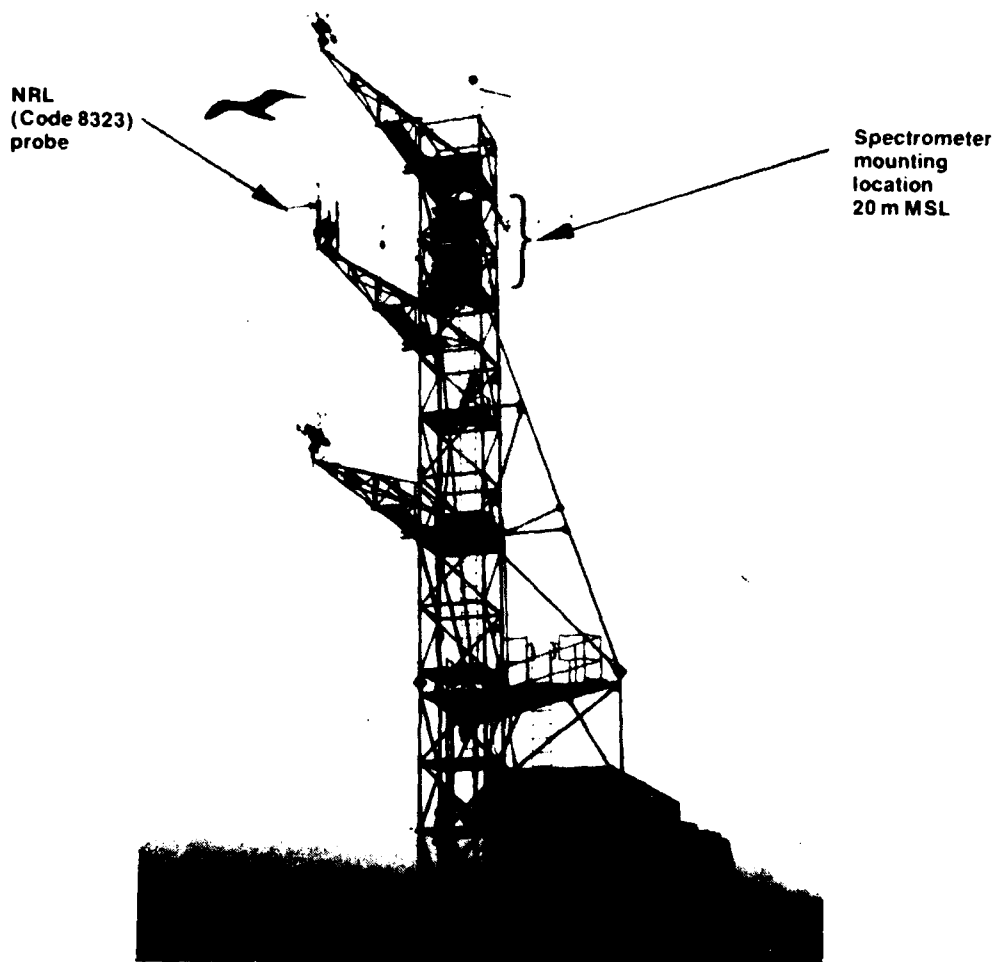

Figure 17. Tower mounting locations of Knollenberg spectrometers at San Nicolas Island.
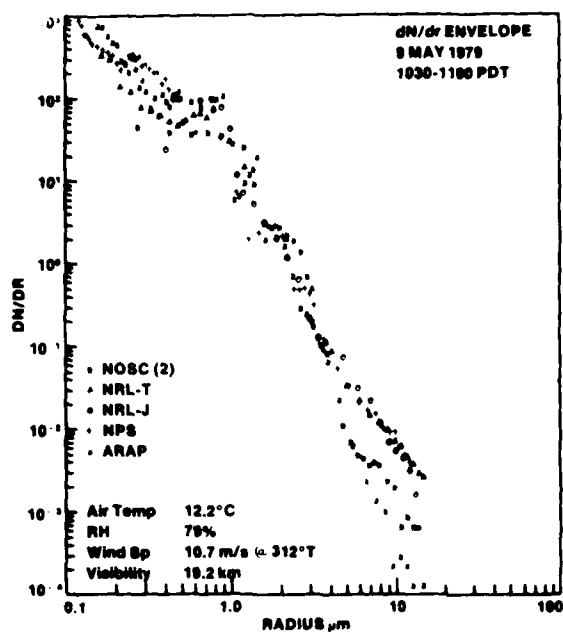
Figure 18.   Aerosol size distributions measured
with different Knollenberg spectrometers during a
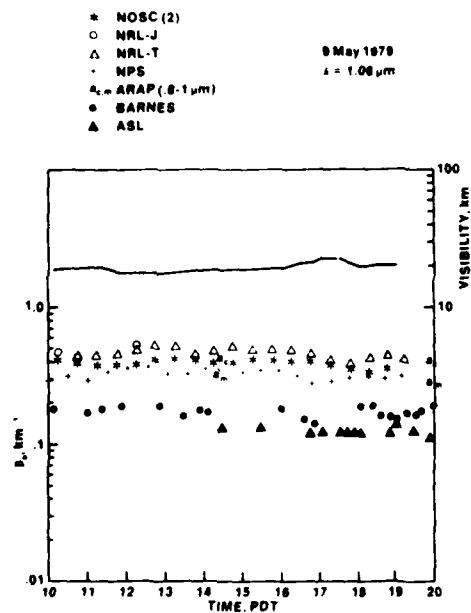30-minute period on 9 May 1979.

Figure 19.   Calculated and measured aerosol
extinction coefficients for 1.06 μm versus time
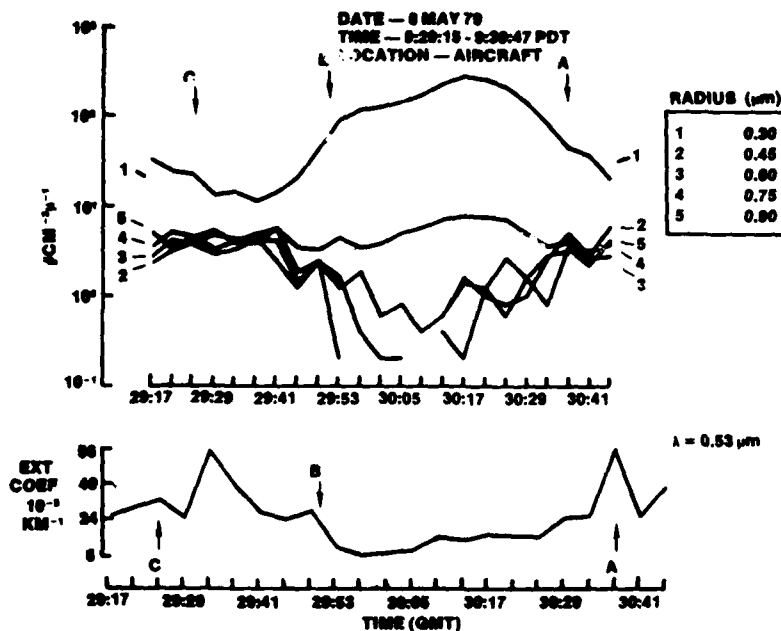for 9 May 1979.

Figure 20. Spatial variation of size distributions and calculated extinction coefficients along the Barnes optical transmission path on 8 May 1979.

(λ = 0.53 μm) as a function of position (time) along the optical path on 8 May. The aircraft flew along the path toward Site A at an elevation of approximately 23 m above the MSL. Between Sites C and B, an increase in β_a was observed (path close to the surf line), corresponding to an increase in the number density of larger particles and a decrease in smaller particles. Over the open water between Sites B and A, the β_a dropped, corresponding to a decrease in the number of larger particles and an increase in the smaller ones. As the aircraft approached Site A, the number density of large particles increased by an order of magnitude, the smaller particle density decreased by the same amount, and, consequently, β_a increased. This path inhomogeneity can partially explain the discrepancies between the end-point extinction coefficients calculated from the Knollenberg data and those measured by the transmissometer and lidar over the optical path. This example illustrates that nonuniform conditions can exist along the SNI optical propagation path (which probably relate to surf and island influences), and

28

caution should be exercised when attempting to validate aerosol distribution models with transmissometer data.

These effects were not encountered during attempts by the Naval Post-graduate School (Fairall, et al, 1980) to compare Knollenberg data with laser transmissometer data at Monterey Bay, California, during the May 1980 Marine Aerosol Generation and Transport experiment (MAGAT-80). In this experiment, four wavelengths in the visible and near-infrared bands were transmitted across a 13.3-km path in Monterey Bay. The research vessel ACANIA (operated by the Naval Postgraduate School) was positioned near the middle of the propagation path, from which aerosol size distributions were made at the same altitude as the optical path. Two Knollenberg probes (CSAS and ASAS) were utilized to measure particles from 0.09-μm to 14.0-μm radius. In figure 21, the extinction coefficients calculated from the measured distributions are compared to those measured at wavelengths of 0.63-μm and 1.06-μm on 5 May 1980. With the exception of two data points, there is excellent agreement between the calculated and measured values over a 20-hour period in which the visibility varied between 15 and 70 km. The high correlation between the Knollenberg and transmission data is further evidenced in figures 22 and 23, where the 0.63-μm and 1.06-μm measured and calculated extinctions, respectively, are compared.

The results of these intercomparison experiments indicate that the Knollenberg aerosol spectrometers generally agree within an order of magnitude and that, for the range of visibilities encountered in the experiment (10-70 km), aerosol model verification by means of these probes may be accomplished to within this order-of-magnitude accuracy. Given this uncertainty in size distributions, the results of the intercomparison experiment indicate that extinction coefficients (depending upon the wavelength band) usually calculated from measured distributions may be considered reliable for model validation to within factors of 2 to 4. Examples of how well the models will predict the variations in extinction with altitude are shown in figure 24

Fairall, C. W., G. E. Schacher, and K. L. Davidson (1980): Atmospheric optical propagation comparison during MAGAT-80, Naval Postgraduate School Technical Report NPS-61-81-002.

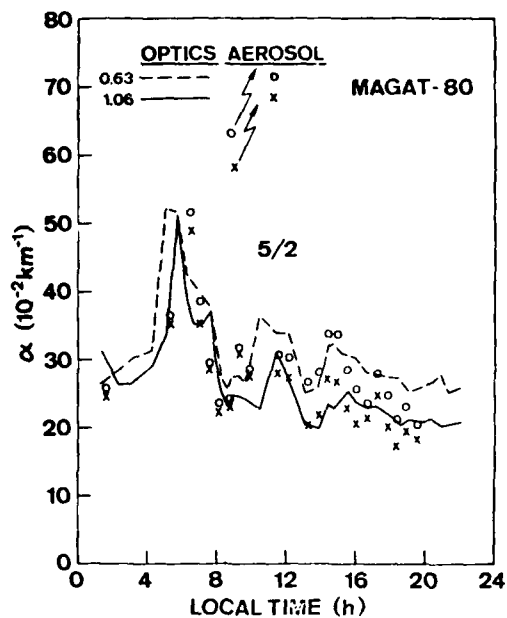Figure 21. Time series plot of aerosol extinction
coefficients from optical transmission
measurements and aerosol size distributions for
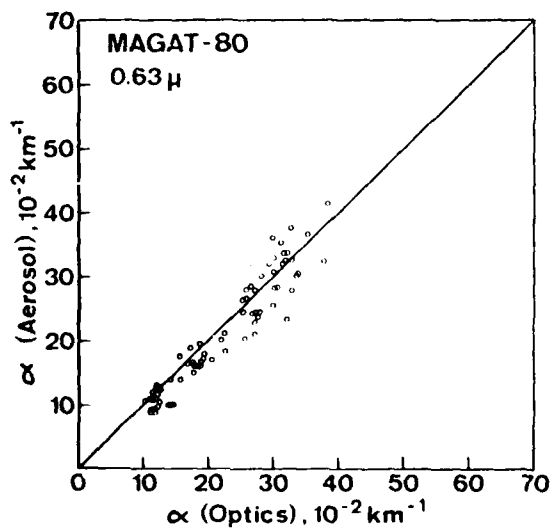0.63 and 1.06 μm.

Figure 22. Comparison of aerosol
extinction coefficients from optical
and aerosol size spectra measure-
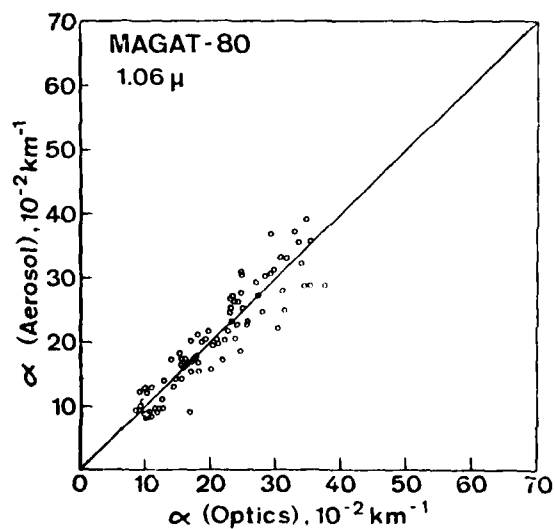ments at 0.63 μm.

Figure 23. Comparison of aerosol
extinction coefficients from optical
and aerosol size spectra measure-
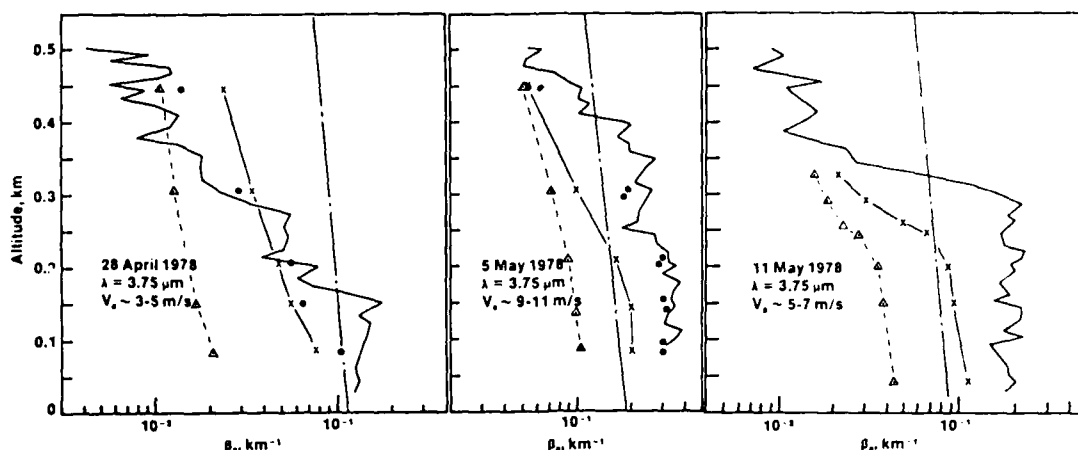ments at 1.06 μm.

30

Figure 24. Aerosol extinction coefficient variations with altitude
calculated by using aerosol size distributions measured during
constant altitude (o) and spiral (————) aircraft flights; the WGM
model (x————x); the LOWTRAN 3B maritime model (——— — ———); and
the K/R (Δ---Δ).

(Hughes, 1980; Hughes and Richter, 1980). In the figure, the extinction
coefficients calculated with altitude by using aerosol size distributions, and
measured by the NOSC aircraft during constant altitude flights and spiral
ascents at sea away from SNI on three different days, are presented. For
these days, the air (T) and dewpoint (T_d) temperatures measured as a function
of altitude, from which the relative humidity (RH) profiles were calculated,
are shown in figure 25. The visibilities used in the LOWTRAN 3B and WGM
models were measured by the Barnes photopic channel at SNI, and the surface
wind speeds used in the WGM and K/R models were measured at the transmiss-
ometer receiver site also at SNI. These data represent (1) a shallow mixed
layer below a weak temperature inversion (28 April); (2) a deep mixed layer
below a strong temperature inversion (5 May); and (3) a shallow mixed layer
below a strong temperature inversion (11 May). In the three data sets the
models agree within a factor of about 2 to 5, with the Knollenberg data at low
altitudes within the mixed layers. The K/R model shows the least agreement,
since it was not scaled to visibility as were the LOWTRAN 3B and WGM models.

Hughes, H.G. (1980): Aerosol extinction coefficient variations with altitude
of 3.75 µm in a coastal marine environment, J Appl Meteor, 19, pp 803-808.

Hughes, H.G., and J.H. Richter (1980): Extinction coefficients calculated
from aerosol size distributions measured in a marine environment, Optical Eng,
19, pp 616-620.

31

Figure 25. Air (T) and dewpoint (T_d) temperature
measured at sea as a function of altitude from
which the relative humidity (RH) profiles are
calculated.

There appears to be little advantage to the WGM model over the LOWTRAN 3B
model at low altitudes within the mixed layers for the visibilities and
wavelength considered here. The major difference between the measurements and
models occurs with the variation in extinction coefficient with altitude above
the mixed layers. This is especially evident in the 11 May data of figure 5,
where there was a strong temperature inversion above the mixed layer which
gave rise to a strong relative humidity gradient between 200 and 400μm. The
WGM model lapse rates follow the Knollenberg data lapse rates better than does
the LOWTRAN 3B model, which is simply scaled exponentially with altitude. For
these types of temperature inversions, where long slant path ranges at sea are
of interest, the users of LOWTRAN 3B stand the risk of underestimating the
range at which a fixed transmittance will occur.

Another apparent deficiency of LOWTRAN is seen in figure 26, where the aerosol extinction coefficients for different wavelength bands (normalized to the photopic band), as measured by the SNI Barnes transmissometer, are plotted versus wavelength for differing visual ranges. Although there is not a constant relationship between the extinction ratio and wavelength for the different visibilities, there is a general trend toward a ratio decreasing with wavelength for increasing visibilities (with the exception of two mid-IR bands for which the trend is reversed to an increasing ratio with increasing visibility). This may be caused by deficiencies in the LOWTRAN-aided water vapor absorption calculations for these bands, which were subtracted from the transmissometer measurements to obtain the aerosol extinction coefficients.
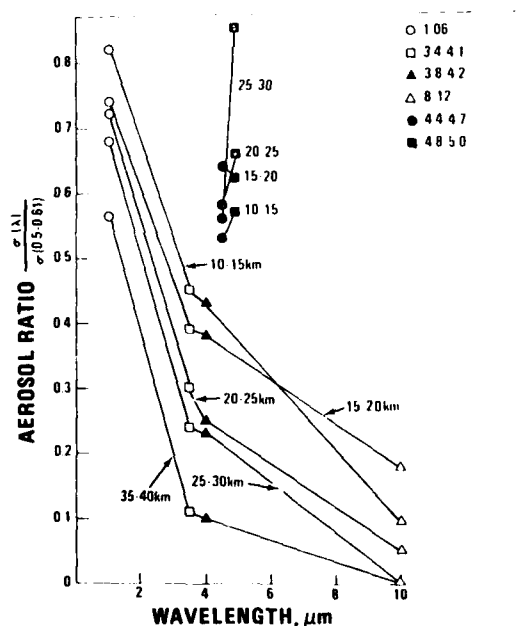

Figure 26. Wavelength dependency for differing
visibilities of experimental aerosol extinction
coefficients for different wavelength bands
(normalized to the photopic band) of the SNI
Barnes transmissometer.

In determining the accuracies with which models can be validated by using measured distributions or transmittances, careful consideration must be given to the effects of meteorological uncertainties used as inputs to the models (Noonkester, 1979). In figure 27, the K/R aerosol size distribution model is compared with the aircraft Knollenberg measurements (curve a) at an altitude of 36 m for a surface wind speed of 6 m/s and measured relative humidity of 93%. The measured distribution is for a 1-minute, 16-second period during a low-level constant altitude flight out to approximately 100 nautical miles from SNI. The surface wind speed is an estimate based on wind speed measurements near Site A on SNI. Curve b does not adequately predict the aerosol number densities, especially in the intermediate and large size ranges. This underestimation in number density may result from the uncertainties in measured relative humidity and surface wind speed used in the calculations. To illustrate the effects of relative humidity, the model is shown for relative humidities of 99% (curve c) and 97% (curve d). The dots show the effect of changing surface wind speed on curve b from 6 m/s to 10 m/s. In general, the model is more sensitive to uncertainties in surface wind speed for relative humidities less than 90%. For values larger than 90%, uncertainties in the humidity are the controlling factors.

This is further illustrated in figures 28 and 29, where the size distributions measured by the NOSC aircraft along the Barnes transmissometer path at SNI are compared with the K/R model for relative humidities less than 90%. In the figures, the surface winds (ws) of 2.9 and 8.75 m/s are 30-minute averages while the aircraft was along the optical path. The aircraft spectrometer data were averages of several flights across the path, as indicated. The aerosol extinction coefficients calculated from the measured modeled distributions are also shown. For the low wind speed, the K/R model underestimates the number density by nearly an order of magnitude for radii between 1 and 3 m. This results in visible, near-IR, and mid-IR extinctions which differ from the measured values near 80%. For the moderate winds, the distributions are in better agreement and the calculated extinctions differ by factors of two to three, which is within the assessment accuracy of the Knollenbergs.

Noonkester, V. R. (1979): Comparison of the Katz-Ruhnke marine aerosol model with spatially distributed data near San Nicolas Island, NOSC TN 679.
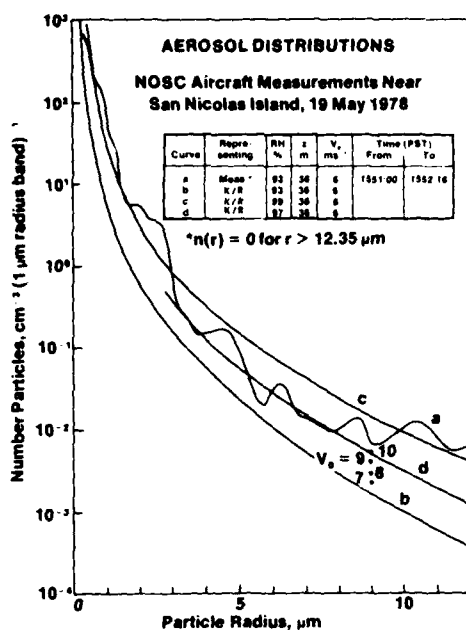
Figure 27. Comparison of aerosol size distri-
butions measured by the aircraft Knollenberg and
those calculated with the K/R model for differing
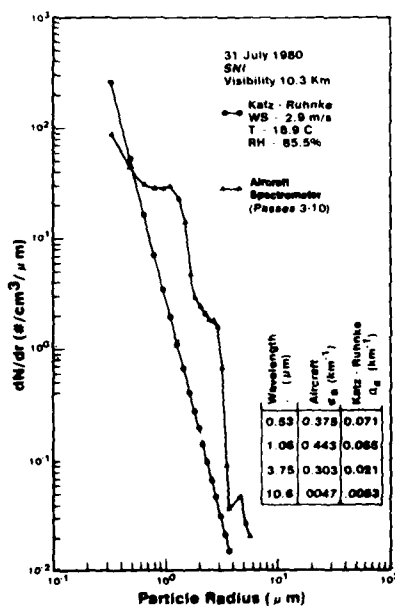relative humidities and surface wind speeds.

Figure 28. Comparison of aerosol size
distributions and extinction coefficients
calculated from aircraft measurements of size
distributions at SNI and the R model for a low
wind speed of 2.9 m/s.

While the aerosol extinction at 10.6 μm is small for both wind speeds, the measured and calculated values differ less than a factor of two. It is interesting to note that while the measured and modeled distributions in figure 28 differ considerably, the extinctions of 10.6 μm are close, which may be because the distribution volumes are controlling factors to extinction. The modeled response of calculated extinction coefficients to surface winds also was investigated by the Naval Postgraduate School during the Joint Air-Sea Interaction (JASIN) experiment between Scotland and Iceland in August and September 1979 (Fairall, 1981).

In figure 30, extinction coefficients calculated at 10.6 μm from the shipboard measurements of aerosol size distributions are plotted versus wind speed and compared with those calculated by using the K/R model for a relative humidity of 87%. While the standard deviations of the extinctions for the measured distributions at constant wind speed are large, the K/R model predicts very well the average values for wind greater than about 7 m/s. Below this value, the model overestimates extinction at 10.6 μm, which is consistent with the aircraft measurements shown in figure 28.

An important and difficult area in model evaluation (and in which less progress has been achieved) is the identification of the appropriate or effective refractive indices of the aerosol that depend primarily on the origin and trajectory of the encountered air masses. The aerosol refractive index is required in Mie calculations of extinction using measured and modeled size distributions, and the Knollenberg calibrations are also fixed for a given refractive index (usually H_2O). While the response of the individual sizing channels can be adjusted for different refractive indices, there is presently no way of knowing the proper values while measurements are being made. If the air mass is of maritime origin, the dry particle can usually be assumed to be NaCl and the effective aerosol refractive index as a function of radius can then be calculated based on growth-rate models which depend upon relative humidity. It is the unknown constituents of the aerosols of con-

---

Fairall, C. W. (1981): Aerosol extinction over the ocean: A field examination of the Wells-Munn-Katz model, BDM Corporation (Monterey, CA) Technical Report BDM/M-TR-0001-81.

22 July 1980
SNI
Visibility 10 4 km

Katz Ruhnke
WS 8 75 m s
T 14.6°C
RH 88.2%

Aircraft Spectrometer
(Passes 1-10)

Wavelength (μm)	Aircraft σ_a (km⁻¹)	Katz Ruhnke σ_a (km⁻¹)
0.53	0.383	0.149
1.06	0.398	0.134
3.75	0.176	0.083
10.6	0.038	0.023

dn/dr (#/cm³/μm)

Particle Radius (μm)

$\lambda = 10.6$ o JASIN   — K/R
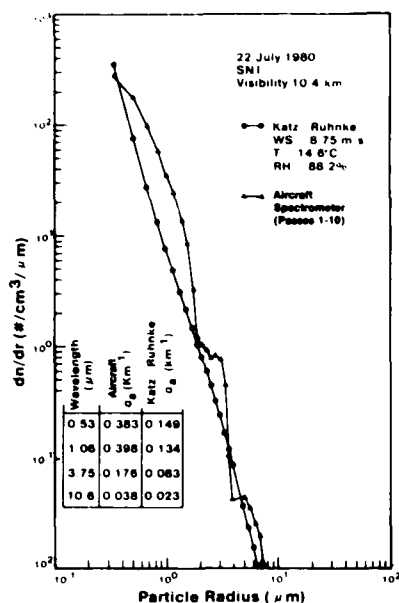
Extinction (km⁻¹)

u (m/s)

Figure 29. Comparison of aerosol size distributions and extinction coefficients calculated from aircraft measurements of size distributions at SNI and the C/R model for a moderate wind speed of 8.75 m/s.
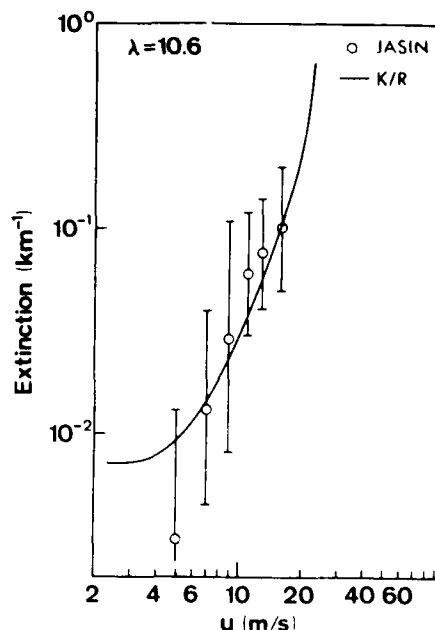
Figure 30. Extinction coefficients for 10.6 μm calculated from aerosol size distributions measured at sea in the North Atlantic and those calculated by using 12-hour averages of measured wind speed.

tinental origin that must be accounted for in model validation attempts. In addition to the refractive index uncertainties, the continental aerosols determine the magnitude of the coefficient of the Junge distribution in the WGM and K/R models.

Recently, some progress has been made in identifying the amount of continental contamination of air masses and their effects on the constants of the size distributions. During CEWCOM-78 (Cooperative Experiment in West Coast Oceanography and Meteorology, May 1978), the Naval Research Laboratory (Larson, 1979) made measurements of atmospheric radon ([222]Rn) at SNI and on board the R/V ACANIA at sea. Measurements of this radioactive gas provide a simple, real-time indicator of the relative maritime/continental nature of the air over coastal areas. Over the land, radon concentrations are of the order of 100 pCi m⁻³; over the ocean, values of 1-4 pCi m⁻³ are typical.

Larson, D. J. (1979): Measurements of atmospheric [222]Rn at San Nicolas Island and over nearby California coastal areas during CEWCOM-78, NRL Memorandum Report 3941.

Radon data collected during May 1978 at SNI and aboard R/V ACANIA are shown in figure 31. The solid line indicates radon concentration measured aboard R/V ACANIA at sea and upwind of SNI. Crosses represent individual samples collected at SNI, and the hatching indicates that the ship was close to the island. The good agreement between island and ship radon data, when they were substantially separated, suggests that large-scale circulations, and hence relatively uniform air, prevailed in the area. The effects of the continental aerosols on the Junge coefficient of the K/R model have been reported by Fairall (1981). Simultaneous measurements of aerosol size distributions were made aboard R/V ACANIA along with the May 1978 radon measurements. The coefficients to the Junge distribution in the K/R model were determined from the distributions measured below 1 µm and are plotted
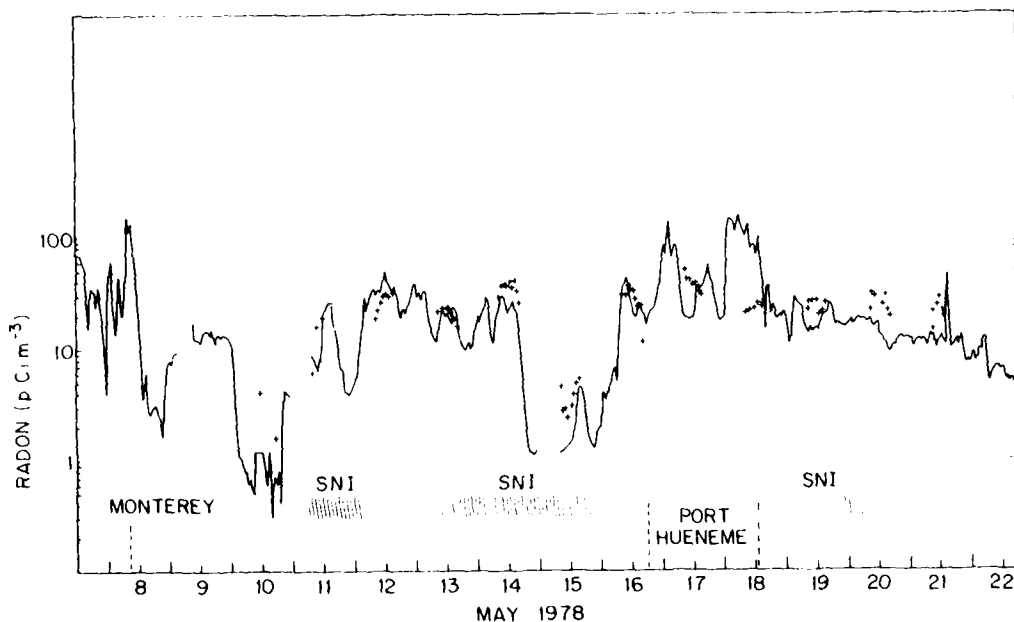
Figure 31. Measurement of radon during CEWCOM-78 at San Nicolas Island and aboard R/V ACANIA (solid line). Crosses represent individual samples collected at the island; the close hatching indicates when the ship was close to the island.

38

versus time in figure 32 along with the radon count. (In this figure, A' is the Junge coefficient normalized by $4\pi/3$.) The strong correlation between A' and the radon count indicates that the Junge coefficient in the K/R model should be varied, depending upon the amount of continental contamination. While ground-based transmissometers and Knollenbergs provide means to validate the aerosol models, their validity with altitude has had only a cursory examination near SNI with the NOSC aircraft Knollenbergs. To augment the aircraft sensors, NOSC has recently (FY80) initiated a program to develop the capability of measuring slant-path transmissions for model comparison and evaluation. Two systems have been designed and assembled, and are still in the process of being evaluated for obtaining reliable slant-path transmission data.

The first of these systems is one which utilizes a RAWIN set (equipment already available) to allow a laser/receiver system to track an optical retroreflector mounted on the NOSC aircraft. A block diagram of the system is shown in figure 33. Basically, the output of a 10-mW HeNe laser is diverged, mechanically interrupted (chopped) at a frequency of 100 Hz, and then deflected such that it is coaxial with a 20-cm-diameter Cassegrain receiving telescope with a silicon diode detector at its focal plane. On aircraft, a 7-cm retroreflector is mounted and manually pointed toward the laser source. The RAWIN set automatically tracks the aircraft by receiving a 1700-MHz rf signal transmitted from a position on the aircraft close to the retro-reflector. To measure the power in the Gaussian-distributed laser beam which is returned to ground, a beamsplitter arrangement is placed in front of the retroreflector such that a portion of the returned laser power is deflected into a radiometer. The laser chopping frequency is used to modulate a 2905-MHz microwave signal on the ground. The signal is transmitted to the aircraft where it is received, demodulated, and used as the reference for synchronous detection of the laser light by a lock-in analyzer, which records its output. The laser signal returned to ground is also synchronously detected by using the same chopping frequency. The range to the aircraft is continuously monitored by a range computer, which measures the phase change of the chopped reference frequency after it has been transmitted to the aircraft and returned to ground. This measurement utilizes a modulation of the 1700-MHz RAWIN tracking signal. With the range to the aircraft and the ratio of
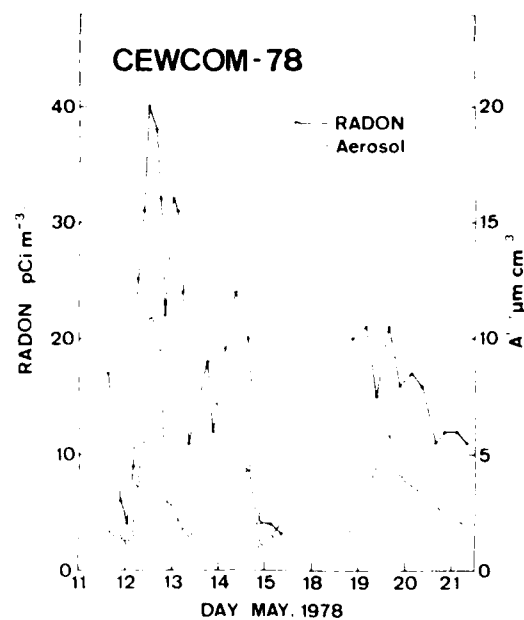
CEWCOM-78

Figure 32. Atmospheric radon activity (solid line) and continental aerosol coefficient (dashed line) during CEWCOM-78.
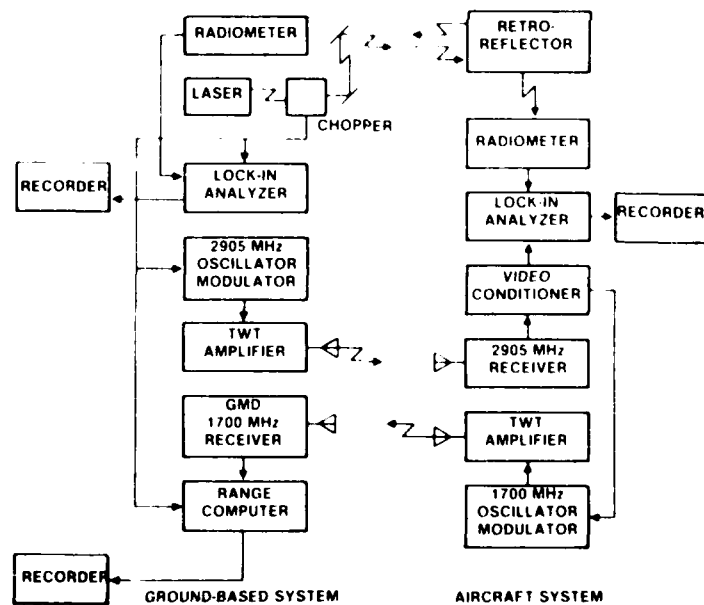
Figure 33. Block diagram of NOSC slant-path laser transmissometer.

the beam powers leaving the retroreflector and received on the ground known, the slant-path atmospheric transmittances and effective extinction coefficients can be calculated. The values can then be used to evaluate the aerosol models based on the meteorological parameters (measured on board the aircraft). The system has been designed and assembled. Clear-air, ground-based calibration factors have been obtained, as well as slant-path data for aircraft altitudes near 300 m and ranges between 2 and 3 km for moderate visibilities.

Because of the physical constraints of mounting a water-cooled CO_2 laser on the RAWIN set, another approach has been taken to determine atmospheric slant path transmissions for infrared wavelengths. This approach has been to fly a thermal imaging system with a calibrated internal temperature reference in a helicopter and thus measure the temperature of ships at sea as a function of range and elevation. The technique requires the assumption that the temperatures and area aspect ratio of the ship remain constant throughout the measurement. The effort is being performed at NOSC with contractual support by Science Applications, Inc, of La Jolla, CA. The thermal imaging system is a Texas Medical Instruments THERMASCOPE model 910B with a spectral sensitivity from 8 to 12 μm. The methodology employed is to record, with a wide field of view on 70 mm film, two different temperatures of the ship's surface at different ranges along a slant path from the ship. The film negative is enlarged and the ship's surface areas are scanned by a microdensitometer. The target temperatures are determined by relating the exposed film densities to a calibration grey scale on the film which is generated by the internal temperature reference. Figure 34 is a photograph of the HALEAKALA (AE-25), an ammunitions ship, taken off Point Loma, CA, with the THERMASCOPE at a range of 200 m from the ship and an altitude of 60 m. In the photograph, "white" is "hot" and the calibration scale to the right corresponds to an 11°C window centered about 14.9°C. It is interesting to note the ship's infrared reflected image on the sea surface. This apparent enlargement of the ship's area should increase the probability of detection at a given range.

By means of the temperature determined from the photographs, it can be shown that the effective extinction coefficient for the band is given by
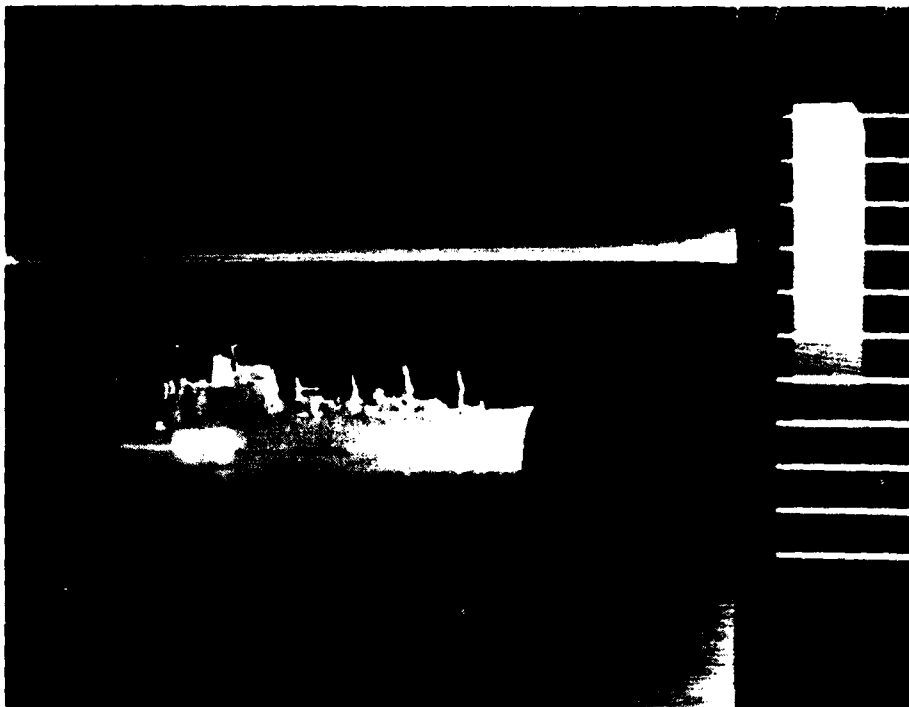
Figure 34. Thermal image of HALEAKALA (AE-25)
taken with helicopter borne THERMASCOPE.

$$\beta_{\Delta\lambda} = \frac{1}{(R_1 - R_2)} \ln \frac{\Delta T(R_1)}{\Delta T(R_2)} \tag{3}$$

where $\Delta T(R)$ is the temperature difference of the ship areas measured at
different ranges R. The slant range to the target is determined by a tri-
angulation technique by using ranges and bearings to the ship and helicopter,
as measured with an X-band radar located on Point Loma. This technique of
temperature difference measurement cancels out the contribution to the
apparent target irradiance from backgrounds and atmospheric emissions along
the path. The molecular absorption contributions to total extinction are then
subtracted from the measured total extinction by LOWTRAN through the use of
the meteorological parameters measured along the propagation path by the NOSC
aircraft. To date, several ship signatures have been obtained for
good-to-moderate visibilities, and the technique is being evaluated by
comparing the measured extinctions with those calculated from the aircraft
Knollenberg measurements.

42

3.3 AEROSOL MODEL DISCUSSION

The results of the Knollenberg intercomparison experiments at SNI have determined the instruments to be valuable tools for assessing electro-optical propagation parameters. While the actual distributions may differ significantly, the extinction coefficients (depending on the wavelength) calculated from the distributions measured with different instruments agree with each other (and with transmission measurements) to within factors of 2 to 4. However, when comparing models with transmission measurements, care should be taken to ensure that the meteorological parameters are representative of the propagation path. Inhomogeneities along the path can greatly affect the aerosol extinctions when molecular calculations from LOWTRAN are used, since they are based on endpoint measurements. From the NPS measurements at Monterey Bay, it can be concluded that midpoint measurements of aerosols and meteorological parameters are to be preferred.

The measurements at SNI have also shown the LOWTRAN 3B aerosol model to be representative of conditions within the mixed portions of the marine boundary layer when good estimates of surface visibility are available and the model agrees well with the WGM. However, the WGM model better describes the conditions above the mixed layer, while LOWTRAN 3B will overestimate extinction. To be equally representative of conditions within the mixed layers, the K/R model needs to be scaled with visibility.

In this paper, considerable emphasis has been placed on the K/R model. This is not to say that it is better than or preferable to the WGM model, but that it has been developed from a different and larger data set and is expected to be better representative of maritime conditions. Past work has shown this model to be a useful tool in climatological studies for wind speeds greater than about 7 m/s. However, considerable refinement of the model is needed before it can be considered useful for operational purposes. In particular, for low wind speeds (RH < 90%), the model underestimates extinction in the visible, near, and mid-IR wavelength bands. This discrepancy may be related to continental influences for which the continental component coefficient may require adjustment as to radon count or even visibility (Fairall, 1981). The model requires more accurate measurements of meteoro-

43

logical parameters (relative humidity and wind speed), surface visibility, and radon count than have been provided up to now. In addition, the model has been evaluated in only a few locations under a limited set of conditions. Very little data are available for evaluation at high wind speeds and high relative humidities. In any event, the model will remain basically the same; that is, it will comprise a continental component and a sea-spray component. Additional empirical data (other than for validation purposes) can be expected to have little impact and should not alter the model. Major changes to the model can be expected to come mainly from first principles; that is, analytical investigations of the boundary layer parameters which control aerosol growth within the convectively mixed layers above the ocean and have not been considered. Of particular concern are the volume of the mixed layer and the effects of cloud coverage and types on the mixing. Certainly, the amount of information and the accuracies required place stringent requirements on the model, and militate against its present use in the real-time assessment of shipboard electro-optical systems performance. For these purposes, alternative methods which directly relate IR extinctions to "simple" scattering measurements (lidars and nephelometers) or aerosol loading parameters (area or volume) may be more appropriate.

4.0 INSTRUMENTATION

The instrumentation development under the Navy's atmospheric transmission effort addresses both atmospheric measurements for model verification and shipboard sensor development for operational applications. The difference between the two is that instrumentation in the research and development effort needs neither to be ruggedized nor to provide real-time data. Both the latter requirements are, of course, mandatory for operational shipboard instrumentation.

A great deal of effort has been spent to calculate, refine, and verify existing instruments for the present purpose. Among these instruments are various particle size measurement (drop size) spectrometers, the Barnes transmissometer, radon counters, nephelometers, and meteorological and micrometeorological sensors. Specifically developed was a new saturation

hygrometer capable of measuring relative humidity between 95%-105% (Gerber, 1980). Figure 35 shows a head-on view (to scale) of the hygrometer sensor head. The hygrometer uses a thin thermal mirror on which condensation is controlled by limiting the exchange of ambient water vapor to condensation sites consisting of submicron-sized salt nuclei. The salt solution droplets formed on the nuclei are prevented from exceeding a reference size by heating the mirror with infrared diodes which are part of a thermo-optic servosystem. The temperature increase of the mirror is directly related to the ambient relative humdity. Measurements of supersaturation in fogs have been success-fully conducted with the instrument (Gerber, 1981).

Another point sensor under development is a rugged nephelometer with dual-cosine sensors. It is designed to measure aerosol scattering coef-ficients at 0.904 µm (GaAs laser-diode source). It is expected to provide an
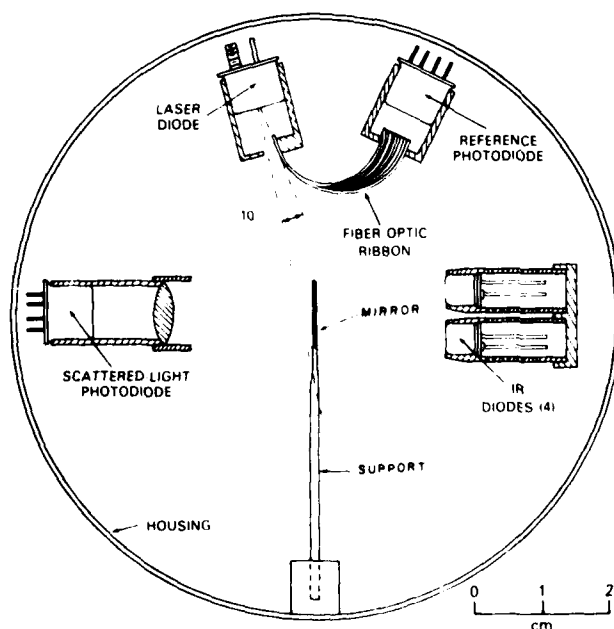

Figure 35. Saturation hygrometer sensor head.

Gerber, H. E. (1980): A saturation hygrometer for the measurement of relative humidity between 95% and 105%, J Appl Meteor, 19, pp 1196-1208.

Gerber, H. E. (1981): Microstructure of radiation fog, J Atm Sci, v 38, pp 454-458.

estimate of visual range and provide a two-parameter fit for the determination of aerosol size distributions.

Since any point sensor measurements may be affected by the measurement location, it is most desirable to utilize remote sensing techniques which also can measure parameters along slant ranges. Lidars are obvious candidates to measure aerosol extinction, which is the most important parameter affecting a broad class of Navy EO systems. For this purpose, a so-called beam image profiling (BIP) lidar was developed by Stokes (1979) and uses geometry to separate atmospheric backscattered light by range rather than time (figure 36). The backscattered laser energy from different range segments is focused to different locations in the receiving telescope's image and measured by a line array of detectors. The instrument was compared by Jensen (1981) to an MRI 1580 visiometer. Figure 37 shows an example of simultaneous measurements during a period of poor visibility. The lidar and the visiometer compare quite favorably, in particular if one considers that the visiometer makes point measurements which may differ from the path measurement by the lidar. Another comparison, this time with visibility calculated from measured drop size distributions, is shown in figure 38. The scatter of the points for higher visibilities can be expected because of the low aerosol concentrations in these cases. Even though data obtained with the BIP lidar are very encouraging, further development of the device was terminated in favor of supporting the Army's conversion of a hand-held laser rangefinder (AN/GVS-5) into a so-called visioceilometer (figure 39) for measurement of visibility and ceiling (Bonner and Lentz, 1978). Initial measurements with this instrument at Meppen, Germany, in fall 1980 and in San Diego in January 1981 gave very promising results. Additional units are being procured for extensive measurements in the whole spectrum of naval environments. The field experience

---

Stokes, R. B. (1979): Beam image profiling (BIP) lidar: design and preliminary evaluation, NOSC TN 782, 28 Sep.

Jensen, D. R. (1981): Atmospheric visibility measurements using a beam image profiling lidar: A final evaluation, NOSC TN 953, 15 Jan.

Bonner, R. S., and W. J. Lentz (1979): The visioceilometer: A portable cloud height and visibility indicator, ASL TR-0042, Oct.
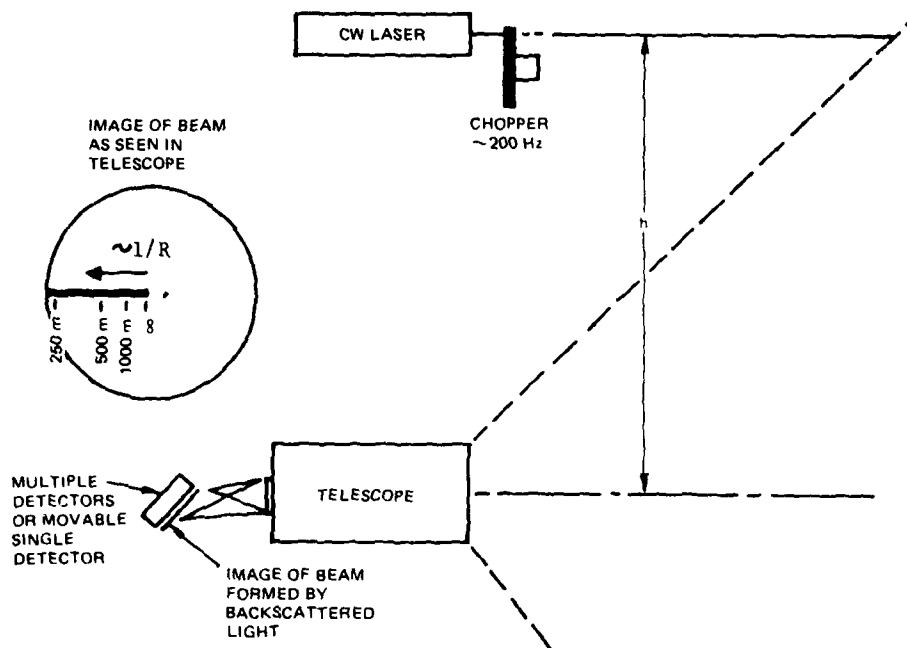
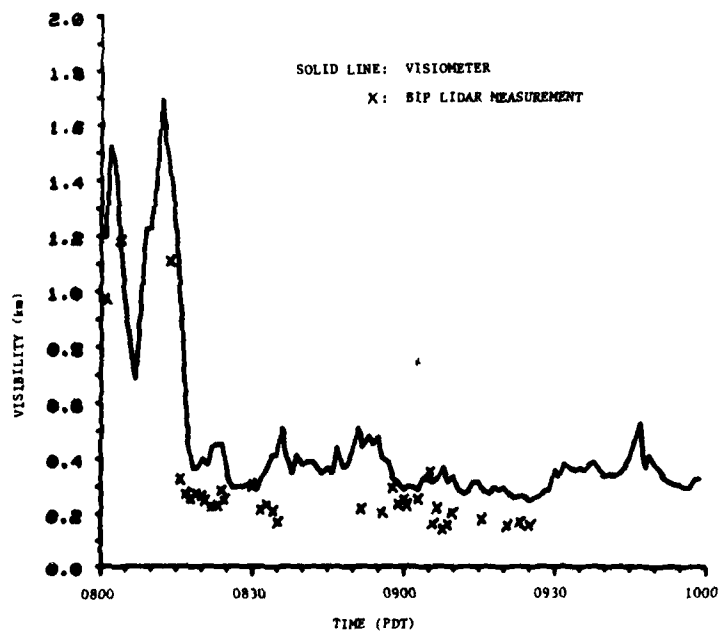Figure 36.   Beam Image Profiling (BIP) lidar.

Figure 37.   Comparison of BIP lidar with the MRI
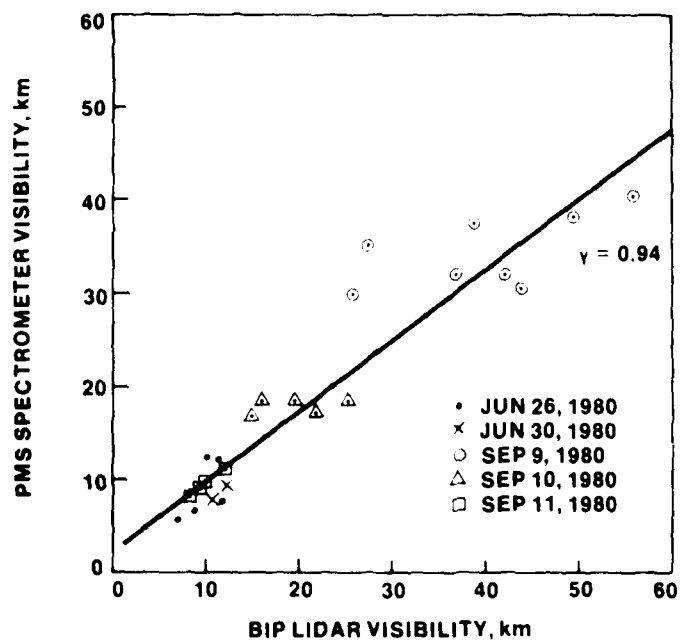1580 visiometer.

Figure 38. Calculated aerosol size spectrometer
visibility versus BIP lidar visibility.

Figure 39. Visioceilometer (modified AN/GVS-5
laser rangefinder).

gained with those visiometers will be used to answer questions like utility of this 1.06-μm unit for estimating visibility, inferring aerosol extinction in inhomogeneous environments, extrapolating results to other wavelength regions, as well as determining reliability, ease of use, and safety of this particular development. Meanwhile, other developments will be followed carefully (eg, laser rangefinders in the eye-safe region) to find the optimum solution in defining the system parameters that will lead (it is hoped) to the development of a triservice atmospheric lidar.

5.0 CONCLUSIONS

The Navy's EO atmospheric transmission program has yielded significant results in the areas of systems performance assessment, worldwide climatologies, aerosol measurement and modeling, and instrumentation development. Future effort will continue in these areas, with an increased emphasis on development of instrumentation for the operational assessment of the propagation environment.

6.0 REFERENCES

Barnhardt, E.A., and J.L. Streete (1970): A method for predicting atmospheric aerosol scattering coefficients in the infrared, Applied Optics, 9, 1337-1344.

Bonner, R.S., and W.J. Lentz (1979): The visioceilometer: A portable cloud height and visibility indicator, ASL TR-0042, Oct.

Deirmendjian, D. (1969): Electromagnetic Scattering on Spherical Polydispersions, Elsevier.

deViolini, R., A. Shlanta, and C.B. Elam (1980): Seasonal cloud amount and cloud free line-of-sight data for the oceanic area off the Somali Coast, PMTC TP 80-19, July.

Fairall, C.W., G.E. Schacher, and K.L. Davidson (1980): Atmospheric optical propagation comparison during MAGAT-80, Naval Postgraduate School Technical Report NPS-61-81-002.

Fairall, C.W. (1981): Aerosol extinction over the ocean: A field examination of the Wells-Munn-Katz model, BDM Corporation (Monterey, CA) Technical Report BDM/M-TR-0001-81.

Fitzgerald, J.W. (1975): Approximte formulas for the equilibrium size of an
aerosol particle as a function of its dry size and composition and the
ambient relative humidity, J Appl Meteor 14, pp 1044-1049.

Gerber, H.E. (1980): A saturation hygrometer for the measurement of relative
humidity between 95% and 105%, J Appl Meteor, 19, pp 1196-1208.

Gerber, H.E. (1981): Microstructure of a radiation fog, J Atm Sci, 38, pp
454-458.

Hitney, H.V., and J.H. Richter (1976): Integrated Refractive Effects
Prediction System (IREPS), Naval Engineers Journal, pp 257-262, April.

Hitney, H.V., and R.A. Paulus (1979): Integrated Refractive Effects Predic-
tion System (IREPS), interim user's manual, NOSC TD 238, March.

Hughes, H.G. (1980): Aerosol extinction coefficient variations with altitude
of 3.75 μm in a coastal marine environment, J Appl Meteor, 19, pp 803-808.

Hughes, H.G., and J.H. Richter (1980): Extinction coefficients calculated
from aerosol size distributions measured in a marine environment, Optical
Eng, 19, pp 616-620.

Jensen, D.R., R. Jeck, G. Trusty, and G. Schacher (1980): Intercomparison of
PMS particle size spectrometers, NOSC TR 555.

Jensen, D.R. (1981): Atmospheric visibility measurements using a beam image
profiling lidar: A final evaluation, NOSC TN 953, 15 Jan.

Junge, C. (1955): The size distribution and aging of natural aerosols as
determined from electrical and optical data of the atmosphere, J Meteor, 16,
pp 654-659.

Katz, B.S., and F.C. DeBold (1981): A statistical evaluation of optical
propagation codes using 1978 San Nicolas Island transmissometer measure-
ments, Proc 29th National IRIS Symposium, Orlando, FL, 19-21 May.

Katz, B.S., F.C. Debold, and J.J. Perez-Esandi (1981): Estimates for the
probabilities of surface-to-air cloud free lines-of-sight and low cloud
statistics at fifteen marine locations from surface observations, NSWC TR
78-143.

Kneizys, F.X., et al (1980): Atmospheric transmittance/radiance: computer
code LOWTRAN 5, AFGL-TR-80-0067.

Larson, D.J. (1979): Measurements of atmospheric ^{222}Rn at San Nicolas Island
and over nearby California coastal areas during CEWCOM-78, NRL Memorandum
Report 3941.

Noonkester, V.R. (1979): Comparison of the Katz-Ruhnke marine aerosol model
with spatially distributed data near San Nicolas Island, NOSC TN 679.

Selby, J.E.A., E.P. Shettle, and R.A. McClatchey (1976): Atmospheric trans-
mittance from .25 to 28.5 μm: Supplement LOWTRAN 3B, AFGL-TR-86-0258.

Snyder, F.P. (1980): PROCAL-PREOS: A fast running airborne FLIR system performance model, NOSC TN 810, 15 Feb.

Stokes, R.B. (1979): Beam image profiling (BIP) lidar: design and preliminary evaluation, NOSC TN 782, 28 Sep.

Wells, W.C., G. Gal, and M.W. Munn (1977): Aerosol distributions in maritime air and predicted scattering coefficients in the infrared, Appl Opt, 16, pp 654-659.